Imperial College London

The Discrete Causal Action and Holes in Spacetime

Joshua Chevalier
Supervised by Fay Dowker

Imperial College London
Faculty of Natural Sciences
Department of Physics
Theoretical Physics Group

Submitted in partial fulfilment of the requirements for the degree of
Master of Science of Imperial College London

Abstract

The Causal Set Program is an approach to quantum gravity which postulates that continuum spacetime is an approximation of a more fundamental structure - a discrete collection of events equipped with a causal order. This work reviews key elements of the program before introducing the Discrete Action on a causal set. The focus of this dissertation is investigating the Benincasa-Dowker Conjecture, which claims that, in the continuum limit, the mean of this action over many 'sprinklings' of a manifold into a causal set gives the Einstein-Hilbert action up to some boundary terms. We introduce a new methodology for calculating the mean action on flat manifolds, and use both this and the old methodology to investigate boundary terms from flat non-globally hyperbolic spacetimes. We provide evidence for various manifolds with and without timelike boundaries. We argue that these results imply that non-globally hyperbolic spacetimes, and in particular spacetimes with holes, are generally suppressed in the path integral over causal sets.

Acknowledgements

I would firstly like to thank my supervisor, Professor Fay Dowker for being an amazing supervisor whose guidance throughout the process of writing this dissertation was invaluable to me. Discussions of how to further my research and how to interpret my results were fascinating to me. I appreciate both the talks, and Fay's wisdom to tell me to stop working and actually write it up.

I would also like to thank my mum for supporting me throughout this last year, as I would not have been able to pursue this master's degree at all if not for her generosity. I would also like to thank my girlfriend, Lauren, for coping with my stress, listening to my crazy thoughts, and making this whole year feel less daunting.

I would finally like to thank my brother, Cameron, for the numerous proof reads of this dissertation he had to endure to get this in shape.

Contents

Chapter 1

Introduction

1.1 Quantum Gravity

The search for a theory of Quantum Gravity (QG) remains one of the most profound challenges for modern physics. General Relativity (GR) and Quantum Field Theory (QFT), although excelling at explaining their respective regimes, have proved individually incomplete when considering the smallest scale and incompatible with each other in the assumptions they make about things as fundamental as time and the topology of the universe.

For the case of GR, we see infinities in curvature $R_{\rho\sigma\mu\nu} = \infty$ at the centre of a black hole and at the big bang. For QFT the problem can be represented by $Z = \infty$, where non-renormalizability becomes a significant issue when trying to quantize the conjectured gravitational gauge boson (the graviton)[1]. At the intersection of the two theories, we have the especially interesting $S_{BH} = \infty$ infinite entanglement entropy of the black hole. The belief that these divergences are not truly physical, but instead are mathematical artifacts of incomplete theories, is one of the primary motivations for quantum gravity.

Conceptually, the problems aren't any easier. General relativity is deterministic, where QFT is inherently probabilistic. GR has no need for an 'observer' nor difficulty asking the question of what is 'measurable', where these questions are central to all of Quantum Mechanics. The backdrop of GR is a dynamic, continuous manifold where matter and energy can influence the curvature. Meanwhile, QFT is formulated on a (usually) flat, fixed backdrop on which fields evolve but which does not evolve itself, and where fields are 'quantized' into discrete packages. Moreover, GR is fundamentally 4 dimensional in that it binds space and time together so tightly that the concept of a 'moment in time' has no meaning [2], whereas QFT is 3+1 dimensional in that we *must* foliate spacetime into fixed moments in time for measurements to make sense.[1] Gravity is also a local theory, as opposed to QM where non-locality is an unavoidable concept when considering phenomena like entanglement. Some, but far from all, of these issues are remedied by taking the 'sum over histories' approach to quantum mechanics

[1]This is made even more problematic when we remember time is one of the things being observed!

over the 'canonical quantization' approach, which we will return to in more detail in later. Refer to [3] for a more in depth discussion of these dichotomies.

To make matters even worse, quantum gravitational effects are only expected to be directly observable near the Planck scale. This is far smaller than current technology has the capacity to probe, with some estimates suggesting that to detect the graviton we would need a collider the mass of Jupiter [4]. Furthermore, the universe seems to have done its best to hide any natural evidence of quantum gravitational effects. Data from the Big Bang, when energies were high enough for QG effects to be significant, may have been 'washed away' by cosmic inflation, and the singularities of black holes are 'clothed' by an observationally impenetrable[2] event horizon.

The current impracticability of testing any proposed theory has led to many competing models - most notably string theory [5] and loop quantum gravity [6] - with mostly only theoretical considerations and an intuition of what the universe 'should' look like to guide them. If there is one test then it is arguably black hole thermodynamics, which has been described as 'the closest thing we have to confirmed results in quantum gravity' [7]. Steven Hawking and Jacob Bekenstein's entropy formula provides a finite answer to the $S_{BH} = \infty$ divergence, but only by introducing a length cut off at the Planck scale [8]. This is roughly the same scale at which we expect our other infinities to emerge and at which we expect quantum gravitational effects to be prevalent. Any successful theory of quantum gravity must reproduce both GR and QFT in their respective regimes whilst also accounting for their failures. The fact that we expect these failures to be roughly at the Planck scale can be seen as indicative that the long accepted 'continuum' on which both QFT and GR are performed is only an approximation of a deeper structure. Could it be that the reason our theories stop making sense at the Planck scale is that it simply isn't physically meaningful to talk about smaller lengths? Could spacetime itself be discrete?

1.2 Overview

The focus of this dissertation is the Causal Set Program, which posits that the Lorentzian manifolds of GR are an emergent approximation of a more fundamental structure - a discrete collection of elements equipped with a causal ordering, called a Causal Set. The discreteness scale is, based on the arguments discussed, expected to be on the order of the Planck length:

$$l_P = \sqrt{8\pi G\hbar} \approx 1.6 \times 10^{-35} m. \tag{1.1}$$

Originally proposed by Bombelli, Lee, Meyer and Sorkin in 1987 [9], Causal Set Theory (CST) has undergone considerable development. The kinematics of the theory are relatively well understood, and there have been exciting recent developments in producing an effective dynamics.

[2] Unless one wanted to fall in to the black hole and take some measurements, but unfortunately the results of those tests would inevitably follow you to the singularity.

The key components of this program are discreteness and causality,[3] which are seen as fundamental.

Causal Set Theory is also associated with one of the most important phenomenological predictions of any theory of quantum gravity: the prediction of the order of magnitude of the cosmological constant [10]. Despite being made from largely heuristic arguments, with a more rigorous causal set dynamics needed to fully justify it, the success of this prediction is one of CST's greatest achievements.

In Chapter 2, we will more rigorously introduce the causal set approach and give an overview of the kinematics of the theory.

In Chapter 3, we introduce two approaches to dynamics. The first are the so called 'bottom up' sequential growth models, which are expected to be the most fundamental approach to dynamics but are as yet not very well understood. The second is a 'top down' approach, in which we define a discrete action on a fixed causal set and use it to investigate dynamics in the continuum limit, thereby acting as an intermediate regime. The focus of this dissertation will be on this approach to dynamics.

Chapter 4, we give a brief overview of how the discrete action is defined, and then introduce the Benincasa-Dowker Conjecture, which posits that the continuum limit of our discrete action gives the Einstein-Hilbert action, up to some boundary terms. We will then discuss what these boundary terms are expected to be, and how they depend on the different assumptions we make about the spacetime we are calculating the action on.

In Chapter 5, we introduce a new methodology for calculating the action on flat manifolds, and introduce the concept of mutual information between spacetime regions.

In Chapter 6, we will calculate the Mean Discrete Action (MDA) on various manifolds with timelike boundaries in order to further probe an as yet relatively unexplored case of the conjecture, providing further evidence that, in this case, the action can be seen to diverge.

In Chapter 7, we will investigate how putting 'holes' in a manifold affects the action on it, providing a partial answer to a problem initially posed by Bombelli [9] in the first paper on causal set theory. We will also discuss how a specific type of 'interval' between two points on a manifold without timelike boundaries might cause its action to diverge.

Finally, in Chapter 8, we summarise our results, discuss how they may be interpreted, and then discuss possible avenues for how research in this direction might be extended.

[3]Motivation for placing such an emphasis on causality can also be drawn from consideration of black holes, where its very definition is given by its causal structure.

Chapter 2

Foundations and Kinematics

A good starting point when introducing Causal Set Theory is defining what a causal set (or 'causet' for short) actually is.

Definition 2.0.1. A causal set is a locally finite partially ordered set. It is a set $\mathcal{C}$ equipped with an order relation $\preceq$ called 'precedes' satisfying the following axioms:

1. **Reflexive:** $\forall x \in \mathcal{C}$, $x \preceq x$.
2. **Antisymmetric:** $\forall x, y \in \mathcal{C}$, if $x \preceq y$ and $y \preceq x$ then $x = y$.
3. **Transitive:** $\forall x, y, z \in \mathcal{C}$, if $x \preceq y$ and $y \preceq z$ then $x \preceq z$.
4. **Locally Finite:** $\forall x, y \in \mathcal{C}$, $|I(x, y)| < \infty$,

where $|I(x, y)|$ denotes the number of elements causally 'between' x and y. Spacetime points are thus represented by elements of $\mathcal{C}$ and the causal structure is encoded by the relation $\preceq$.

Formally, $I(x, y) := \{z \in \mathcal{C} \mid x \prec z \prec y\}$ where we define that $x \prec y$ if and only if $x \preceq y$ and $x \neq y$.

$|I(x, y)|$ denotes the cardinality of that subset.

This the clear analogue of the Alexandrov interval in general relativity, $A[x, y]$, which is the intersection of the future light cone of x and past light cone of y, for some causally related points x, y in Lorentzian manifold $\mathcal{M}$. Explicitly $A[x, y] := \mathcal{J}^+(x) \cap \mathcal{J}^-(y)$ where $\mathcal{J}^\pm$ is the causal future(+) / past(-). This is also known as a *causal diamond*.[1]

The first three axioms of definition 2.0.1 define a partially ordered set (or poset) and are in agreement with the expected causal relationships on Lorentzian manifolds. The local finiteness condition encodes the desired 'discreteness' into our structure, and allows us to assign a 'volume' to a subset $\mathcal{C}' \subset \mathcal{C}$ by just counting the number of elements in that subset: $\mathrm{Vol}(\mathcal{C}') = |\mathcal{C}'|$.

[1]The terms Alexandrov interval, causal interval, and causal diamond will be used interchangeably.

2.1 How is a causal set a manifold?

The justification that enough information is encoded in these axioms to reproduce the topology, metric, and differentiable structure of a continuum spacetime is founded in theorems by Hawking [11] and Malament [12], which were then later extended by Levichev [13], and most recently Parrikar [14]. These show that the entire geometry of a (past and future distinguishing) d-dimensional manifold $(\mathcal{M}, g)$ is encoded by its causal structure - up to its *volume element* $\sqrt{-g}d^d x$. This missing piece cannot be reproduced from the causal order alone. We could write this result as something like:

$$\text{Causal Structure} + \text{Volume Element} = \text{Lorentzian Geometry}.$$

For a causal set, its causal structure is encoded in our order relation, and the missing volume element is conveniently provided by its discreteness as simply the number of elements in a given region. This fantastic result motivates Sorkin's 'slogan' for CST:

$$\text{Order} + \text{Number} = \text{Lorentzian Geometry}.$$

Placing causality as fundamental means any manifold produced from a causal set *must* have a Lorentzian metric and henceforth all manifolds discussed are assumed to be Lorentzian unless otherwise stated.

2.2 When is a causal set a manifold?

While we know that a causal set *can* encode all the information to reproduce the geometry of a manifold, this is clearly not true for all causal sets.[2] We need a notion of *when* we can say that a given spacetime $(\mathcal{M}, g)$ can be seen as an approximation of a causal set $(\mathcal{C}, \preceq)$. To do this we need a faithful embedding:

Definition 2.2.1. A *faithful embedding* of a causal set $(\mathcal{C}, \preceq)$ into a Lorentzian manifold $(\mathcal{M}, g)$ is a map $f : \mathcal{C} \to \mathcal{M}$ preserving causal structure such that,

$$x \preceq y \in \mathcal{C} \iff f(x) \preceq f(y) \in \mathcal{M},$$

and such that the image $f(\mathcal{C})$ is uniformly distributed in $\mathcal{M}$ with respect to its volume measure. In this context we define that $x \preceq y \in \mathcal{M}$ if and only if $x \in \mathcal{J}^-(y)$.

By uniformly distributed we mean that the number of elements embedded in any given region of the manifold depends only on the volume of the region.

Definition 2.2.2 (Manifold-like)**.** A manifold $(\mathcal{M}, g)$ is said to be 'a good approximation' of a causal set $(\mathcal{C}, \preceq)$ if there exists a faithful embedding from $\mathcal{C}$ to $\mathcal{M}$. The causal set can then be called *manifold-like*.

[2] A single element by itself fulfils the axioms of a causet.

For this to be useful, and for the idea that spacetime is emergent from a causal set to have any merit at all, we cannot have vastly different manifolds approximating the same causal set. This leads us to the 'Hauptvermutung' or central conjecture of CST:

Conjecture 2.2.1 (Hauptvermutung)**.** If a causal set $(\mathcal{C}, \preceq)$ can be faithfully embedded into two Lorentzian manifolds $(\mathcal{M}, g)$ and $(\mathcal{M}', g')$, then the two manifolds are 'approximately isometric'.

Here 'approximately isometric' roughly means that the manifolds can differ at scales smaller than the embedding scale. As discussed, in causal set theory our discreteness scale is the Planck length, so manifold's whose geometry differs only at levels smaller than the Planck scale can be approximations of the same causal set. This is fine as we don't expect these scales to be physically meaningful.

This conjecture is not proven, and indeed a large part of the problem is defining rigorously what this 'approximately isometric' actually means. [15]. However, the Hauptvermutung is supported by a large and growing body of evidence, which comes in the form of finding 'order invariants' on a manifold-like causal set which limit to manifold invariants in the continuum approximation. Such results include dimension [16][17], distance [18][19], topology [20], and curvature [21].

2.3 Which causal sets are manifolds?

While we now have a definition for whether a given causal set is 'manifold-like', it is practically very difficult to determine when this is the case. Furthermore, we also have the problem that the vast majority of causets are highly non-manifold-like. The most significant entropic contribution to the sample space Ω of causal sets comes from a specific class of non-manifold-like causets called the Kleitman-Rothschild (KR) causets, consisting of only three 'moments in time'. Given a random n-element causal set, the probability of it being a KR causet actually goes to 1 as $n \to \infty$ [22].

For CST to be a successful theory we must recover general relativity in the continuum limit, therefore manifold-like causets are the only ones we want to consider. We thus have two questions:

1. How can we overcome the domination of non-manifold-like causal sets to the entropy of the sample space?

2. How can we find the manifold-like causal sets which we hope to consider?

The answer to the first question we hope lies in the dynamics, which we will return to later. The answer to the second question is a method for constructing causal sets corresponding to a given manifold called *sprinkling*.

Sprinkling

The idea of a sprinkling is that we generate our causal set by simply picking a subset of points from a given manifold $\mathcal{M}$ and appending them to a causal set $\mathcal{C}$, along with inherited order relations $\preceq$ from the causal structure of the manifold. The preservation of causal structure means that any $\mathcal{C}$ constructed this way is embeddable in $\mathcal{M}$, but there is subtlety in how we must pick our points. For this to be a *faithful* embedding the image $f(\mathcal{C})$ must be uniformly distributed in $\mathcal{M}$. A tempting but misguided approach is to fix a Lorentz frame, split $\mathcal{M}$ into a lattice, and pick points regularly along it. In this frame, $f(\mathcal{C})$ would (naïvely) be uniformly distributed in $\mathcal{M}$. However, by boosting our frame we would effectively 'stretch out' our lattice such that it was no longer uniform. By picking points in this way we would have unintentionally produced a causal set approximated by a manifold without isotropy!

We thus need to find some process of picking points that preserves Lorentz invariance. The answer to this turns out to be a *Poisson process*. By randomly sprinkling our points according to a Poisson distribution, we have that the probability of picking n points from a region of $\mathcal{M}$ with volume V is:

$$P_n(\rho, V) = \frac{(\rho V)^n}{n!} e^{-\rho V}, \tag{2.1}$$

where ρ is a parameter called the *density* of the sprinkling. On average, the number of points in a volume V is then given by $\langle N \rangle = \rho V$.

While a Lorentz transformation on such a configuration would still change its microstate, its macroscopic properties are unchanged in that we still have our uniform distribution of $\langle N \rangle = \rho V$. We could say that our transformed configuration is 'equally random'. By picking our points this way, we have ensured that our embedding is faithful and that the resultant manifold will be Lorentz invariant.

It is important to note that we can take many different sprinklings of the same manifold $\mathcal{M}$. Clearly, sprinkling at different densities will produce causal sets with different cardinalities, and they will each be 'approximately isometric' to $\mathcal{M}$ at different embedding scales. More than this, due to the random nature of sprinkling we can produce many different causal sets from the *same* density of sprinkling! In this sense there is a whole class $[\mathcal{C}(\mathcal{M}, \rho)]$ of causal sets that can be faithfully embedded in $\mathcal{M}$ at embedding scale ρ. This is not at odds with the Hauptvermutung, which says that the same causal set cannot approximate two distinct manifolds, not that a manifold cannot be approximated by different causal sets. In line with the Hauptvermutung we could define the class of manifolds which are approximately isometric above some scale ρ as $[\mathcal{M}_\rho]$ and summarise this result as: '$[\mathcal{C}(\mathcal{M}, \rho)]$ is well approximated by $[\mathcal{M}_\rho]$'.

Coarse Graining

It has been shown that there are some small causal sets which *cannot* be embedded in d-dimensional Minkowski space $\mathbb{M}^d$ [17]. This is problematic as this means

that by rearranging a small number of points in a manifold-like causal set we can make it unembeddable. As we would like a theory that is invariant under small quantum fluctuations, this indicates that the condition for a causal set to be approximated by a manifold may be too strong. Instead, it may be that the fundamental structure of spacetime is non-manifold-like, but we may regardless recover the continuum by in some sense 'zooming out'. For $\rho < \rho'$ we can see $\mathcal{C}(\mathcal{M}, \rho)$ as a 'zoomed out' version of $\mathcal{C}(\mathcal{M}, \rho')$. In analogy with this, for a large, non-manifold-like causet $\mathcal{C}'$, it sometimes possible to find some subset $\mathcal{C} \subset \mathcal{C}'$ such that $\mathcal{C}$ is well approximated by some manifold $\mathcal{M}$ even though $\mathcal{C}'$ is not. The process of finding such a subset is called *coarse graining*.

2.4 Representations and Analogues

While for most of this text we will be working in the continuum limit, it will be useful going forward to have some visualisation of what a causal set might look like on the scale of elements. We will also introduce some terminology and causal set analogues to spacetime structures.

Hasse Diagrams

A given causal set is entirely described by its elements and its order relations, but for large causets it would be extremely tiresome to explicitly and exhaustively write out every single order relation. Instead, diagrammatic representations of causal sets called Hasse Diagrams are often employed.

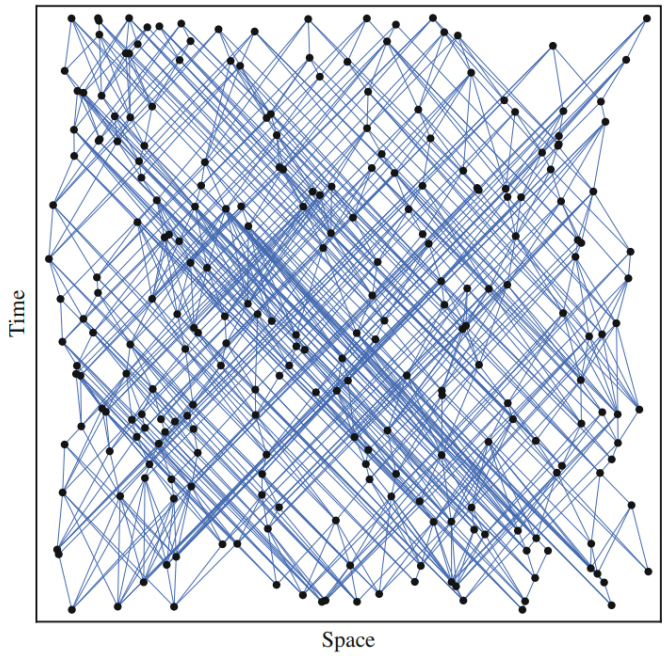

Figure 2.1: The Hasse Diagram of a causal set generated by sprinkling into $\mathbb{M}^2$. Image credit [7].

In these diagrams, each point corresponds to an element of the causet, and the lines represent the causal structure. As we see in Figure 2.1, the only causal relations drawn are *links* between 'causally adjacent' elements, where we interpret the lower of the two points of the link to 'precede' the upper point. We can infer all other causal relations from transitivity.

Terminology

For a given Causal Set $\mathcal{C}$ we can define the following:

Definition 2.4.1 (Link)**.** A *link* is an irreducible order relation between two elements of $\mathcal{C}$. Formally, for any $x, y \in \mathcal{C}$, we say that there is a link between x and y if $x \prec y$ and there exists no $z \in \mathcal{C}$ such that $x \prec z \prec y$. We denote this $x \prec\!* \, y$.

Definition 2.4.2 (Ancestor and Descendent)**.** If $x \prec y$ then we say that y is a *ancestor* of x and that x is a *descendant* of y.

Definition 2.4.3 (Past and Future)**.** The *future* of x is the set of all descendants of x, $\text{Future}(x) = \{y \in \mathcal{C} \,|\, x \prec y\}$. The *past* of y is the set of all ancestors of y, $\text{Past}(y) = \{x \in \mathcal{C} \,|\, x \prec y\}$. We can then give an equivalent definition for the causal interval as $I(x, y) = \text{Future}(x) \cap \text{Past}(y)$.

Definition 2.4.4 (Chain and Path)**.** A *chain* is a subset of $\mathcal{C}$ such every pair of elements is causally related. An *n-chain* is a chain consisting of exactly n elements. A *path* is a chain such that no element has more than one link to its past or to its future.

Definition 2.4.5 (Antichain)**.** An *antichain* is a subset of $\mathcal{C}$ such that each element is causally unrelated to each other. An *inextendable antichain* is an antichain that is maximal in $\mathcal{C}$, i.e. we can add no more elements of $\mathcal{C}$ to it and it remain an antichain.

Analogues

A chain is the analogue of a timelike path in GR, and an obvious question is how might we expect a particle to move along such a path. In GR, particles follow geodesics and their future is determined by their initial position and velocity. However, in CST, non-locality means that we cannot exactly define the velocity of a particle at a given point, and particles are expected to be subject to random acceleration called *swerves* away from the geodesic.[3] These swerves have astrophysically testable phenomenology and have been investigated in the context of explaining high energy cosmic rays [23].

The analogue to a spacelike hypersurface[4] in GR, is an inextendable antichain $\mathcal{A} \subset \mathcal{C}$. By its definition, all other elements of $\mathcal{C}$ must lie either in the past or

[3]The analogue of a timelike geodesic in CST is the *longest* chain between two points.

[4]This is an example of a 'Moment in Time Surface' for globally hyperbolic spacetimes.

future of $\mathcal{A}$. However, unlike spacelike hypersurfaces, this is not equivalent to decomposing the space into a past and future due to the presence of 'missing links' which bypass the antichain. If we identify $\mathcal{A}$ as the 'present time' then these missing links would be equivalent to a past event influencing a future event without ever being in the 'present'. As a result, defining a 'fixed time' required by the Hamiltonian in the canonical approach to quantum mechanics is not possible and instead the 'sum over histories' interpretation is needed [24]. While not perfect, our analogue is still useful, and a process of 'thickening' an antichain $\mathcal{A}$ (which itself contains no causal relations and hence no information other than its cardinality) by adding elements near its past an future, can be seen as a rough analogue of taking a time-measurement [25].

Chapter 3

Dynamics

So far we have described what a Causal Set *is* and how we might hope to recover a continuous spacetime from it. We now need a model for how things might *change* on a causal set. Without such a notion, our causet would produce a spacetime which looked just like a manifold but where there were no equations of motion and nothing could ever happen.

It will first be useful to describe the setting on which we want our dynamics to take place. This is the set of causal sets, or sample space Ω. Whether we consider all causal sets in that sample space depends on the situation. When modelling the beginning of the universe we only want to consider past finite causets, whereas when investigating the discrete action it is convenient to restrict to sets with a fixed number of elements [24]. While it would be extremely convenient to restrict our sample space to only manifold-like causal sets, there is no a-priori reason to do so, and we instead hope that the unwanted non-manifold-like causets dynamics will be suppressed by the dynamics.

As we want to reproduce quantum mechanics, we ultimately expect the dynamics on Ω to be governed by some 'quantum measure' μ. In contrast with classical measure theory, we must we replace the 'countable additivity' axiom of the probability measure with a 'quantum sum rule' [26]. This is due to interference between histories, and such a measure is necessary for governing transition amplitudes in quantum sequential growth models. Unfortunately, quantum measure theory is still very much in its infancy, and even if we had a covariant, causal quantum measure we may still not be able to interpret it [27]. As such we need to start with a simpler case.

3.1 Classical Sequential Growth

The most notable successes in building a first principles dynamics[1] for CST are the sequential growth models. In particular, the stochastic *Classical Sequential Growth (CSG)* model, as first proposed by Sorkin and Rideout [28], has been an

[1]This method of working only from the fundamental causal relations is the so called 'bottom up' approach.

important step. Roughly speaking, the idea of these is to 'grow' a causal set, element by element, in a process that follows certain rules. On our sample space Ω, we define a natural partial order by saying one causet $\mathcal{C} \in \Omega$ is related to another causet $\mathcal{C}' \in \Omega$ if $\mathcal{C} \subset \mathcal{C}'$. This partial order of causal sets is called the *Poscau*.

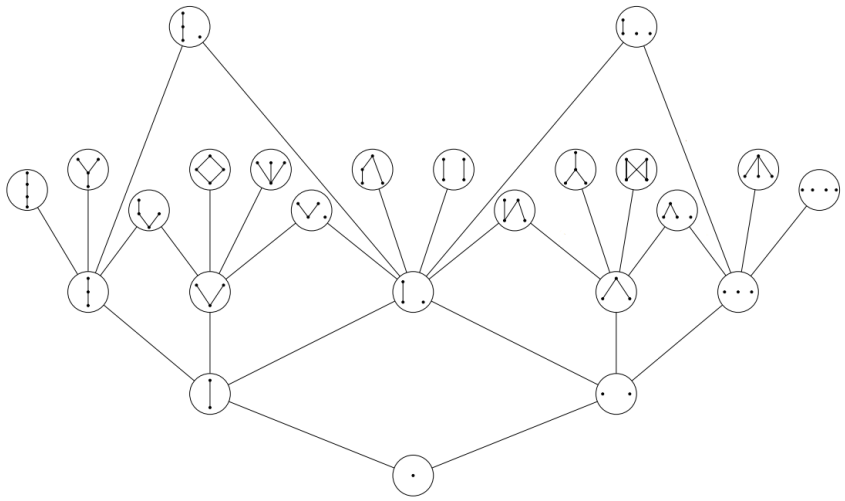

Figure 3.1: A representation of the Poscau, including all causal sets of cardinality up to four, along with their order relations. Image Credit: [29].

The Poscau can be represented by a 'Hasse diagram of Hasse diagrams', as shown in Figure 3.1, explicitly showing the relations. Starting from a single element,[2] we can 'grow' a causet by moving in 'stages' along the Poscau, with a new element being 'born' into the causet at each stage, with some transition probabilities of where to add it with respect to the other elements. The rules that describe where this can be are summarised as:

Definition 3.1.1. (Transition Rules of CSG) [30]**.**

1. **Internal Temporality:** New elements cannot be born to the past of an existing element.

2. **General Covariance:** The probability of reaching a given causal set should only depend on the start and end point of the Poscau. In other words it should not matter which order elements are born.

3. **Markov Sum rule:** A new element must always be born. The sum of probabilities of where to place an element in the next stage of the Poscau must be unity.

4. **Bell Causality:** The probability of a new element being placed at a given point in a causal set depends only on the elements in the past of that point.

[2]Note that we can start from any size causet, but starting from one is most demonstrative.

The 'birth' of each new element can be understood in this context as the passage of time, which is an interpretation enforced by condition of internal temporality. General covariance is the causet equivalent of diffeomorphism invariance. The condition of Bell Causality, named after the paradoxically non-local Bell inequalities, enforces a sense of locality to the growth. Philosophically, this picture of accumulating events feels more natural as a reflection of how we perceive time than the 'Block Universe' of GR [27]. Even with these restrictions, there is still a large choice of growth parameters which result in different causal sets, and without borrowing concepts from the continuum we can proceed no further. However, this has not prevented further insights being drawn from these models.

It has been shown that, in a universe evolved from this model, every element must have a descendant [31]. As such, the causal set will always continue to grow, even after an extreme collapse such as the big crunch or at the centre of a black hole, in a phenomenon dubbed as 'Causal Immortality' [32]. In line with this idea, certain choices of parameters have yielded causal sets reminiscent of 'Big Bounce' cosmologies [33]. In this situation, there is a continual cycle of growth and collapse, where after each 'big bang' after a collapse we will have a new 'renormalised' set of parameters. From this perspective, the answer to the fine-tuning problem could potentially lie in some kind of cosmological natural selection [34], or simply in the fact that there have been so many cycles that eventually some universe had to be conducive to life.

It has also been shown that, while causal sets produced by these models are generally non-manifold-like, they are nothing like KR causets [30]. This is significant as 'proof of concept' that the entropic domination of non-manifold-like causets to the sample space can be overcome by dynamics as hoped. While we must wait for an accepted quantum measure theory in order to have a good chance at formulating a *Quantum Sequential Growth* model, this is a promising start.

3.2 Continuum Dynamics

In contrast to the microscopic dynamics of sequential growth, we will now consider an 'intermediate regime' of effective quantum dynamics based on the sum over histories (SOH) approach to quantum mechanics. While less rigorously developed than the canonical approach (which has been shown not to make sense from the causal set perspective), the SOH approach promises to remedy many of the conceptual issues that the canonical quantization brings [35], and was one of the original motivations for CST [9]. Despite the incompatibility of the fundamental dynamics with this approach, we hope that, as we move towards the continuum limit,[3] the dynamics will start to resemble a path integral.

When formulating CST as a path integral, each causal set acts as a history

[3]Strictly we speak only of a a continuum 'approximation' but we will use the terms interchangeably in this context.

with which we associate some complex amplitude. The partition function is then:

$$Z \equiv \sum_{\mathcal{C} \in \Omega_n} e^{\frac{i}{\hbar} S(\mathcal{C})}, \tag{3.1}$$

where Ω_n is the sample space of all causets of cardinality n and $S(\mathcal{C})$ is some discrete action on a causal set. The best candidate for this, and an important development for CST, is the discrete Benincasa-Dowker (BD) Action which we will introduce shortly.

In order to recover GR from this the action, $S(\mathcal{C})$, must be 'slowly varying' near the solutions to the Einstein Field Equations (EFE), and 'quickly varying' elsewhere [29]. The principal behind this idea is the stationary phase approximation, which is a well-regarded and widely used heuristic argument in quantum mechanics. Here is the concept as presented by Richard Feynman [36]:

> "Suppose that for all paths, S is very large compared to $\hbar$. One path contributes a certain amplitude. For a nearby path, the phase is quite different, because with an enormous S even a small change in S means a completely different phase - because $\hbar$ is so tiny. So nearby paths will normally cancel their effects out in taking the sum - except for one region, and that is when a path and a nearby path all give the same phase in the first approximation (more precisely, the same action within $\hbar$). Only those paths will be the important ones."

This idea will be important in how we interpret our results later on.

There is hope that through this mechanism, and other path integral techniques, we will be able to suppress not only non-manifold-like causets but also undesirable spacetimes.

For the former there has been success in using the discrete action to show that a class of non-manifold-like 'bilayer causets' is suppressed in the path integral.[4] Although this is a smaller class than the dominant KR causets, it is still much larger than the set of manifold-like causets and there is hope of generalising the result [37].

To address the latter it is worth asking what we mean by an 'undesirable spacetime'. Clearly we want solutions of GR, but there is a sense in which this is insufficient. As pointed out in [27], spacetimes with boundaries or holes[5] are perfectly good solutions to the EFE, and the fact that we have not observed holes or boundaries in spacetime is not accounted for by GR. This problem was also acknowledged in the original paper on CST [9].

To make matters worse from a GR perspective, it is not clear what spacetimes we should consider 'physically reasonable'. In [38], the conditions of *inextendability*,

[4]This was shown using the Saddle Point Approximation, which is a technique often used when dealing with sharply peaked integrals with dominant contributions coming from the complex plane.

[5]Note that we are **not** referring to black holes which are just points of infinite curvature.

isotropy, *global hyperbolicity*, and *hole-freeness* were listed as the most common assumptions for an acceptable universe, but these cannot be taken as axiomatic and are largely motivated by philosophical considerations. Another condition, proposed by Hawking, for a spacetime to be considered physically reasonable is *causal continuity*, which informally is the condition that as you move around a manifold, your causal past shouldn't be able to suddenly change as a new region of a manifold is made accessible or inaccessible to you [39].

While we expect the fundamental structure to be the Causal Set, these considerations are important as we hope to use what we know about the continuum in order to draw insight in CST, rephrasing these GR concepts in terms of causets to produce a dynamics.

The effect of dropping some of these conditions on the action of a spacetime, and hence contribution from that type of spacetime to the path integral, is heavily explored in Chapters 4 through 8.

Before we can do this, however, we must introduce what the action on a causal set actually is.

Chapter 4

Action and Conjectures

4.1 The d'Alembertian

The first step towards a causal set action is defining a discrete d'Alembertian on a fixed manifold-like causal set.

The continuum d'Alembertian, $\Box$, is a local differential operator, and as such its definition at a given point $x \in \mathcal{M}$ relies finding the limit of some quantity as the distance between x and its 'nearest neighbours' $y \in \mathcal{M}$ goes to zero. This is at odds with the fundamental nature of CST which has been shown to be radically non-local on the Planck scale.

To demonstrate this, we consider a sprinkling into infinite Minkowski space $\mathcal{C}(\mathbb{M}^d, \rho)$. The CST analogue of 'nearest neighbours' is links but, considering the causal future of any $x \in \mathcal{C}$, any elements 'hugging the light cone' will be only one Planck unit of time apart from x, and hence linked to x, however spatially separated it is. Every x is therefore linked to infinitely many other elements of $\mathcal{C}$. This non-locality is an unavoidable result of having a theory which is both discrete and Lorentz invariant [40].

In order to recover locality in the continuum limit, these non local contribution must in some sense cancel each other out.

The first proposal for a discrete d'Alembertian was given for a causal set approximated by 2D Minkowski space [41][42], and was later generalised to a d-dimensional family of operators [21][43].

The 2D discrete d'Alembertian for a function $\phi : \mathcal{C} \to \mathbb{R}$ is given by:

$$\hat{B}^{(2)}\phi(x) := \frac{1}{l^2}\left(-2\phi(x) + 4\sum_{y\in L_0(x)}\phi(y) - 8\sum_{y\in L_1(x)}\phi(y) + 4\sum_{y\in L_2(x)}\phi(y)\right), \tag{4.1}$$

for any $x \in \mathcal{C}$, and where l is some length. The sets $L_k(x)$ are defined as the set of elements $y \in \mathrm{Past}(x)$ such that $|I(x,y)| = k$, i.e. there are k elements strictly between x and y. For a non-manifold-like causet, the factor of $\frac{1}{l^2}$ is just so that $\hat{B}^{(2)}\phi$ has the correct dimensionality, and the value of l is unimportant. However,

for a two dimensional manifold-like causet $C(\mathcal{M}, \rho)$, we must use $l = \rho^{-\frac{1}{2}}$.

While we could, in theory, apply this operator to any real-valued function on any causal set, it was constructed with the continuum in mind, and the coefficients are designed such that we will reproduce the continuum d'Alembertian for a 2D manifold-like causal set. The fact that this is an alternating sum gives indication into how the non-local contributions might cancel each other out.

To investigate how successful this is, we would like to show that, given some scalar field on a manifold, $\phi : \mathcal{M} \to \mathbb{R}$, the value of $\hat{B}^{(2)}\phi(x)$[1] for a corresponding sprinkled causal set, $\mathcal{C}$, is close to $\Box\phi(x)$ for any given point $x \in \mathcal{M}$.[2] For any ρ, we have a whole class $[\mathcal{C}(\mathcal{M}, \rho)]$ of causets which are well approximated by $\mathcal{M}$, each generally giving a different value of $\hat{B}^{(2)}\phi(x)$. While the variance between the values of $\hat{B}^{(2)}\phi$ for different sprinkling is very important, we would also like to define a quantity that depends only on the manifold, scalar field, and sprinkling density.

For this purpose, we associate a random variable $\hat{\mathbf{B}}^{(2)}$ to each class $[\mathcal{C}(\mathcal{M}, \rho)]$ based on the *probability* of finding some value of $\hat{B}^{(2)}\phi(x)$ when we randomly generate a sprinkling. We are then interested in the *expected value* $\langle\hat{\mathbf{B}}^{(2)}\phi(x)\rangle$.

In fact, we indeed find that the non-local contributions cancel out and the limit of the expected value is:

$$\lim_{\rho\to\infty}\langle\hat{\mathbf{B}}^{(2)}\phi(x)\rangle = \Box\phi(x), \tag{4.2}$$

for $\mathcal{M} = \mathbb{M}^2$ and provided ϕ is of compact support with x not on the past boundary of that support [44]. We can similarly define a discrete d'Alembertian, $\hat{\mathbf{B}}^{(4)}$, for which we find an equivalent result for $\mathcal{M} = \mathbb{M}^4$ [21].

By recovering the continuum d'Alembertian we have restored a sense of locality to CST. It is noteworthy that this locality is not expected to fully persist as we continue to increase the scale and, in fact, this 'cosmic non-locality' is interpreted as the source of dark energy [41].

Under certain additional assumptions to ensure that the non-local contributions do not contribute in the limit, this result can be generalised to arbitrary dimension and curvature. We find, for a d-dimensional manifold $\mathcal{M}$ with Ricci scalar $\mathcal{R}(x)$, that:

$$\lim_{\rho\to\infty}\langle\hat{\mathbf{B}}^{(d)}\phi(x)\rangle = \Box\phi(x) - \frac{1}{2}\mathcal{R}(x)\phi(x), \tag{4.3}$$

where $\hat{\mathbf{B}}^{(d)}$ is the d-dimensional discrete d'Alembertian [45].

[1] For the sake of brevity, we are using ϕ for both the scalar field on $\mathcal{M}$ and the corresponding function on $\mathcal{C}$. In the latter case, we really mean $\phi \circ f$, where f is a faithful embedding of $\mathcal{C}$ into $\mathcal{M}$.

[2] To ensure $x \in \mathcal{M}$ is in the sprinkled causal set, we can just add it by hand.

4.2 The Action

Equation 4.3 shows us that our $\hat{\mathbf{B}}^{(2)}$ operator is not generally the d'Alembertian, but instead actually encodes the curvature of the space. In fact, if we substitute $\phi(x) = -1$ into equation 4.3 then we see that the RHS is $\frac{\mathcal{R}(x)}{2}$. To consider the LHS, we substitute $\phi(x) = -1$ into equation 4.1, and identify:

Definition 4.2.1 (Discrete Ricci Scalar)**.**

$$R^{(2)}(x) := \frac{1}{l^2}\left(4 - 8N_0(x) + 16N_1(x) - 8N_2(x)\right), \tag{4.4}$$

where $x \in \mathcal{C}$ and $N_k(x) = |L_k(x)|$.

In analogy with the Einstein-Hilbert Action:[3]

$$\frac{1}{\hbar}S^{(d)}_{EH} := \frac{1}{l_P^{d-2}}\int_{\mathcal{M}} d^dx\sqrt{-g}\,\frac{1}{2}\mathcal{R}(x), \tag{4.5}$$

we sum over all elements in the causal set to define:

Definition 4.2.2 (2D Benincasa-Dowker Action)**.**

$$\frac{1}{\hbar}S^{(2)}(\mathcal{C}) \coloneqq \sum_{x\in\mathcal{C}} l^2\frac{1}{2}R^{(2)}(x) = 2N - 4N_0 + 8N_1 - 4N_2 \tag{4.6}$$

where $N = |\mathcal{C}|$, $N_k = \sum_{x\in\mathcal{C}} N_k(x)$.
The length l^2 can be seen as an analogue to the volume element $d^2x\sqrt{-g}$, and we notice that the prefactor of l_P^{2-d} seen in the Einstein-Hilbert action is equal to unity in two dimensions. Also note that the action is dimensionless, as we would expect.

The *variance* between the value of the action on different sprinklings of a manifold is very important to the path integral. We expect that physically unreasonable manifolds will have large variance and hence there will be large oscillations when integrating over the different sprinklings, causing them to cancel each other out. However, we again seek a quantity that does not depend on our specific choice of sprinkling.

The *Discrete Action* is given by the random variable $\hat{\mathbf{S}}^{(2)}_\rho$ associated with the probability of getting a specific value of $S^{(2)}(\mathcal{C})$ for a random sprinkling $\mathcal{C}(\mathcal{M},\rho)$. Remembering Equation 2.1, the probability of picking k points from a region of $\mathcal{M}$ with volume V with is:

$$P_k(\rho, V) = \frac{(\rho V)^k}{k!}e^{-\rho V}.$$

The expectation of this random variable is then given by:

$$\frac{1}{\hbar}\langle\hat{\mathbf{S}}^{(2)}_\rho(\mathcal{M})\rangle = 2\langle N\rangle - 4\iint \rho^2 P_0(\rho, V_{xy}) + 8\iint \rho^2 P_1(\rho, V_{xy}) - 4\iint \rho^2 P_2(\rho, V_{xy})), \tag{4.7}$$

[3]This is the cosmological convention.

where integral bounds and volume elements have been omitted for brevity, and V_{xy} is the volume of the causal interval, $A[x,y] = \mathcal{J}^+(x) \cap \mathcal{J}^-(y)$. The bounds and volume elements are explicitly shown in Equation 4.9.

These integrals are the continuum equivalent of summing over the L_k sets, as in Equation 4.1. We see that the coefficients are exactly as in the 2D Action.

Expanding out, we have that:

$$\frac{1}{\hbar}\langle \hat{\mathbf{S}}_\rho^{(2)}(\mathcal{M})\rangle = 2\rho V - 4\rho^2 \iint \left(e^{-\rho V_{xy}} - 2(\rho V_{xy})e^{-\rho V_{xy}} + \frac{(\rho V_{xy})^2}{2} e^{-\rho V_{xy}} \right), \tag{4.8}$$

where $V \coloneqq \mathrm{Vol}(\mathcal{M})$, and we recall that $\langle N \rangle = \rho V$. To make this more concise, we define an operator $\hat{\mathcal{O}}_2 \coloneqq 1 + 2\rho\frac{d}{d\rho} + \frac{1}{2}\rho^2\frac{d^2}{d\rho^2}$. We then write the action, now explicitly showing the integral bounds and volume elements, as:

Definition 4.2.3. (2D Mean Discrete Action (MDA)) [46][4]**.**

$$\frac{1}{\hbar}\langle \hat{\mathbf{S}}_\rho^{(2)}(\mathcal{M})\rangle = 2\rho V - 4\rho^2 \int_{\mathcal{M}} d^2x\sqrt{-g(x)} \int_{\mathcal{M}\cap\mathcal{J}^+(x)} d^2y\sqrt{-g(y)}\hat{\mathcal{O}}_2 e^{-\rho V_{xy}}, \tag{4.9}$$

We note that this can be formulated for general dimensions $d \geq 2$, but $d = 2$ and $d = 4$ are the most explored.

We will give a more detailed discussion of the properties of this action and ways to calculate it later. First, we want to know to what extent this is similar to the Einstein Hilbert Action.

Conjecture 4.2.1 (Benincasa-Dowker Conjecture)**.** The continuum limit of the MDA, for any spacetime in d dimensions, is the Einstein Hilbert action S_{EH} *up to some boundary terms* [44].

4.3 Boundary Terms

The specific form of the conjecture is dependent not only on the type of boundaries we see in the manifold, but also on more general properties like global hyperbolicity, causal convexity, and causal discontinuity. To properly structure an investigation of the boundary terms of the action under different assumptions about $\mathcal{M}$, we split the problem into cases.

4.3.1 Globally Hyperbolic Spacetimes

The first is the case that $\mathcal{M}$ is globally hyperbolic and of finite volume. This is the most explored case, and we have seen that global hyperbolicity is one of the most common assumptions for a 'physically reasonable' spacetime.

[4]Note that [46] differs from the correct action by a renormalisation factor of 2.

In this case, the boundary $\partial\mathcal{M}$ will be *achronal*, meaning that it is nowhere timelike.[5] We can therefore split the boundary into a past and future $\partial\mathcal{M} = \Sigma_- \cup \Sigma_+$, where $\Sigma_\pm$ is defined as the subset of $\partial\mathcal{M}$ through which all future(+)/ past(−) directed causal curves must leave $\mathcal{M}$.[6]

The conjecture in this case is:

Conjecture 4.3.1 ($\mathcal{M}$ Globally Hyperbolic)**.**

$$\lim_{\rho\to\infty} \frac{1}{\hbar}\langle \hat{\mathbf{S}}^{(d)}_\rho(\mathcal{M})\rangle = \frac{1}{l_P^{d-2}}\left(\int_{\mathcal{M}} d^dx\sqrt{-g(x)}\frac{\mathcal{R}}{2} + \mathrm{Vol}_{d-2}(J)\right), \tag{4.10}$$

where $J := \Sigma_- \cap \Sigma_+$ is the *joint* and $\mathrm{Vol}_{d-2}(J)$ is its (co-dimension 2) volume [44].

Evidence

There is considerable evidence for Conjecture 4.3.1. Much of this evidence is given for the case of the Alexandrov interval $\mathcal{M} = A[p, q]$.

When $p, q \in \mathbb{M}^d$, the joint for an interval of timelike height[7] τ is a $(d-2)$-sphere, S_{d-2}, of radius $\frac{\tau}{2}$. It was shown in [47] that, for all dimensions up to $d = 16$, the action on $\mathcal{M}$ has the expected joint term $\mathrm{Vol}(J) = (\frac{\tau}{2})^{d-2}S_{d-2}$. In 2D, this joint contribution presents itself as $\mathrm{Vol}(S_0) = 2$. This is independent of the size of the interval, as first derived in [46], where the conjecture was also shown to hold for the flat 2D triangle and cylinder.

The conjecture has been further supported by calculations for manifolds with curvature. In conformally flat spacetime the expected contributions were found for the diamond in two and four dimensions, and for the 2D slab and triangle [48]. There is also evidence in the case of small causal diamonds with arbitrary curvature [49].

The Joint Interpretation

The interpretation for why we get this joint contribution is motivated by the invariance of the action under order reversal. The argument made in [48] goes as follows:

In Equation 4.1 in our derivation for the action, we defined $L_k(x)$ such that it counted order relations to the *past* of x. Doing it this way is called the *retarded* formulation. However, we could have equally defined $L_k(x)$ to count order relations to the *future* of x, which is called the *advanced* formulation.

In the retarded formulation, we argue that any x with at least three order relations preceding it, as used for the 2D action (Equation 4.6), will provide the 'correct' contribution to the action. As $\rho \to \infty$, the only elements which will not

[5]Note that while finite volume and global hyperbolicity implies achronality, the reverse is not true.

[6]We can also define these in the presence of timelike boundaries but their union will not give the whole of $\partial\mathcal{M}$.

[7]Timelike height means the proper time between event p and event q.

provide the correct contribution are those on the past boundary Σ_- as there is no 'space' under those elements.

Similarly we can argue that in the advanced case it is only the elements on the future boundary which do not give the correct contributions. However, as the action is invariant under changing formulations, we argue that the only elements that potentially give the 'wrong' contribution are those in both Σ_+ and Σ_-, i.e. the joint. It is argued that the elements here in some sense do not have enough space to behave correctly.

Boundary Terms for GR

In general relativity we must also consider boundaries. When formulating the Einstein Hilbert action on a manifold with a boundary we must include a Gibbons Hawking York (GHY) boundary term to ensure we yield the correct field equations [50]. While, from Conjecture 4.3.1, we don't expect the MDA to include spacelike boundary contributions, there has been success constructing a causal set analogue that approaches the spacelike GHY term in the continuum limit [47]. Furthermore, connections have been made between the joint contribution and a certain formulation of the GHY null boundary term [51]. These results help further the assertion that the MDA truly corresponds to the Einstein Hilbert action.

From here on, we shall only consider manifolds that are subsets of Minkowski space $\mathcal{M} \subset \mathbb{M}^d$.

4.3.2 Non-Globally Hyperbolic Spacetimes

For the case that $\mathcal{M}$ is not globally hyperbolic, the situation is more complicated as we must now consider regions which are not causally convex. To formally define causal convexity, we need to define a new type of causal interval.

So far, our definition of $A[x, y]$ has enforced that it is a subset of $\mathcal{M}$. It will be useful to define a new causal interval $\tilde{A}[x, y]$ for any two points $x, y \in \mathcal{M}$, which is just the normal causal interval when we treat x and y as points in $\mathbb{M}^d$.

This can include points outside of $\mathcal{M}$, in the ambient Minkowski space (see Figure 4.1). We then have that $A[x, y] = \tilde{A}[x, y] \cap \mathcal{M}$, and we can now define causally convex:

Definition 4.3.1 (Causally Convex)**.** Let $\mathcal{M} \subset \mathbb{M}^d$, then we say that $\mathcal{M}$ is *causally convex* if, for any $x, y \in \mathcal{M}$, we have that $\tilde{A}[x, y] \subset \mathcal{M}$.

So, a manifold is not causally convex if some causal curve can leave it and come back in, as shown in Figure 4.1. We can then define the *poke-over* as the subset $\tilde{A}[x, y] \backslash A[x, y]$. We denote the volume of the poke-over region by θ_{xy}.

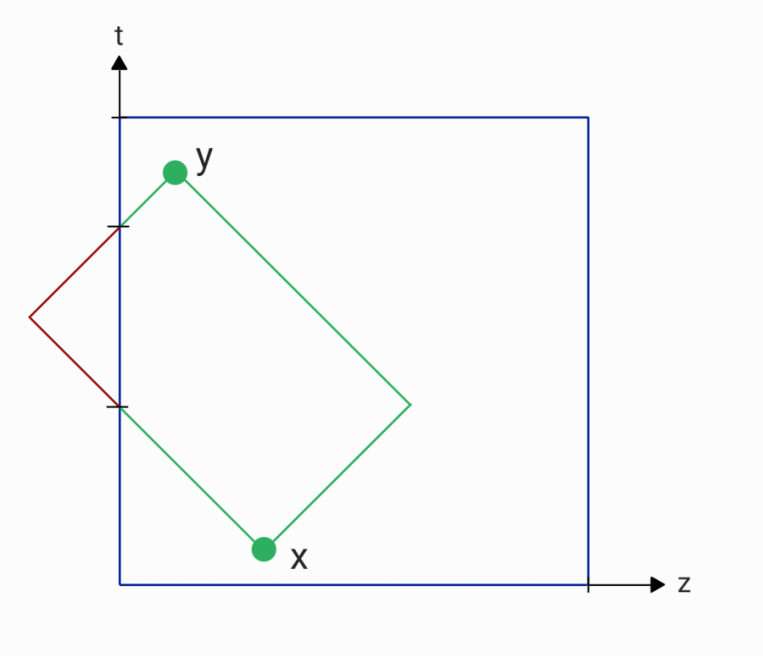

Figure 4.1: A causally non-convex region labelled with Cartesian coordinates. A causal interval $A[x, y]$ is shown, bounded by the green line and the t-axis. The corresponding interval $\tilde{A}[x, y]$ is the region bounded by the green and red lines.

With this in mind, when considering some causally non-convex region $\mathcal{M}$ we may make one of two assumptions:

Definition 4.3.2 (Regimes)**.**

1. We consider causal sets $\mathcal{C}$ sprinkled from $\mathbb{M}^d$. When defining the action we then define a *link* $(x \prec * y)$ to be such that x and y are both in $\mathcal{M}$ and $\tilde{I}(x, y)$[8] $\subset \mathcal{C}(\mathbb{M}^d, \rho)$ is empty. When deriving the MDA this way we use $V_{xy} = \text{Vol}(\tilde{A}[x, y])$, which does include the volume of the poke-over. We interpret this as the manifold actually being embedded in Minkowski space, and call this the *embedded regime*.

2. We consider causal sets $\mathcal{C}$ sprinkled *only* from $\mathcal{M}$. When defining the action we then define a *link* $(x \prec * y)$ to be such that x and y are both in $\mathcal{M}$ and $I(x, y) \subset \mathcal{C}(\mathcal{M}, \rho)$ is empty. When deriving the MDA this way, we use $V_{xy} = \text{Vol}(A[x, y])$, which does not include the volume of the poke-over. We can interpret this as the manifold being all that there is, with no ambient region for causal curves to pass through. We call this the *isolated regime*.

Timelike boundaries

Numerical simulations have indicated that for flat 2D manifolds with timelike boundaries the action will diverge in the continuum limit [44]. We make a conjecture for each regime:

[8]We define $\tilde{I}(x, y)$ analogously to $\tilde{A}[x, y]$.

Conjecture 4.3.2 (Timelike Boundaries)**.** For any 2D Lorentzian manifold $\mathcal{M}$ in the presence of timelike boundaries of total timelike length T, we have that:

(a) Embedded Regime:

$$\lim_{\rho\to\infty} \frac{1}{\hbar}\frac{1}{\sqrt{\rho}}\langle \hat{\mathbf{S}}^{(2)}_{\rho}(\mathcal{M})\rangle = a_0 T. \tag{4.11}$$

(b) Isolated Regime:

$$\lim_{\rho\to\infty} \frac{1}{\hbar}\frac{1}{\sqrt{\rho}}\langle \hat{\mathbf{S}}^{(2)}_{\rho}(\mathcal{M})\rangle = b_0 T, \tag{4.12}$$

where a_0 and b_0 are dimensionless constants.

We thus expect the action to diverge as $T\sqrt{\rho}$ in both regimes, but with a different prefactor in each case. We note that while Conjecture 4.3.1 was made for general dimensions, due to lack of evidence we only make these conjectures in 2D. This is relatively unexplored in either regime as the presence of timelike boundaries means the integral must be split into many parts depending on relative position of x and y, making them quite complicated. We will see in Chapter 6 that calculations are especially difficult for the isolated regime. In that chapter, for the flat 2D case, we will provide analytic evidence for Conjecture 4.3.2(a) and numerical evidence Conjecture 4.3.2(b).

Non-Timelike Divergence

A manifold can fail to be globally hyperbolic without timelike boundaries. Examples of these are the 'Null Doughnut', 'L-Piece' and 2D 'flat trousers', which will be discussed in depth in Chapter 7. A result for the flat trousers in [46] found that the action diverged as $\log\rho$, but there is no pre-existing conjecture associated to regions of this form and as such we will save further remarks for later.

Chapter 5

Properties of the action

Now we have some indication of what results we *expect* to get for a given manifold, let's discuss some properties of the action and how we actually *test* it.

For the purposes of making calculations clearer later on, let's break down Definition 4.2.3 into more manageable parts.[1] We will also simplify our notation for the 2D MDA on some manifold $\mathcal{M}$ by dropping the prefactor of $\frac{1}{\hbar}$, referring to it simply as $\langle S(\mathcal{M})\rangle$, and defining:

$$Y_\rho(x) \coloneqq \int_{\mathcal{M}\cap\mathcal{J}^+(x)} d^2y\sqrt{-g(y)}e^{-\rho V_{xy}}, \tag{5.1}$$

$$X_\rho \coloneqq \int_{\mathcal{M}} d^2x\sqrt{-g(x)}Y_\rho(x). \tag{5.2}$$

We then have that:

$$\begin{aligned}\langle S(\mathcal{M})\rangle_{xy} &= 2\rho V - 4\rho^2\hat{\mathcal{O}}_2\int_{\mathcal{M}} d^2x\sqrt{-g(x)}\int_{\mathcal{M}\cap\mathcal{J}^+(x)} d^2y\sqrt{-g(y)}e^{-\rho V_{xy}}\\ &= 2\rho V - 4\rho^2\hat{\mathcal{O}}_2\int_{\mathcal{M}} d^2x\sqrt{-g(x)}Y_\rho(x)\\ &= 2\rho V - 4\rho^2\hat{\mathcal{O}}_2 X_\rho,\end{aligned} \tag{5.3}$$

where we notice that $\hat{\mathcal{O}}_2$ is independent of x and y, and hence the operator can be applied before or after either of the integrals. The subscript xy indicates that the action was calculated integrating over y and then x.

The $\hat{\mathcal{O}}_2$ operator can be seen as killing off certain powers of ρ to avoid divergences[2], and its location in a calculation can have practical effects on how easily Mathematica can evaluate certain integrals. We call this method of integrating y and then x the *standard method*.

From a functional perspective, the calculation of X_ρ for a given manifold $\mathcal{M}$ is simply the integral of $e^{-V_{xy}}$ over all pairs of causally related points $x, y \in \mathcal{M}$.

[1] Many texts will break the MDA down into $\langle\hat{\mathbf{S}}(\mathcal{M})\rangle = \int_{\mathcal{M}} L_\rho(x)$. We break it down a slightly different way as this is more fitting with a different technique for calculating the action that will be introduced later.

[2] It can be easily seen that ρ^{-1} and $\rho^{-\frac{1}{2}}$ are annihilated by $\hat{\mathcal{O}}_2$.

Once we have X_ρ, the rest of the pieces essentially boil down to regulating the divergence to produce the right limit.

A key point moving forward is noticing that there are actually many ways we could integrate over all causally related points $x, y \in \mathcal{M}$, and hence finding X_ρ, which do not require us use the standard method.

An obvious other approach is to swap the order of the x and y integrals and instead calculate:

$$X_\rho = \int_{\mathcal{M}} d^2y \sqrt{-g(y)} \int_{\mathcal{M}\cap\mathcal{J}^-(y)} d^2x \sqrt{-g(x)} e^{-\rho V_{xy}}, \tag{5.4}$$

which we will call the *reverse method*. However, there is little reason to believe that calculating the integral this way would have any practical advantages over the standard method.

5.1 The Diamond

For a quick example of how the MDA can be calculated using the standard method we will re-derive the result for the 2D flat causal diamond $\diamond = A[p, q] \subset \mathbb{M}^2$, as seen in Figure 5.1.

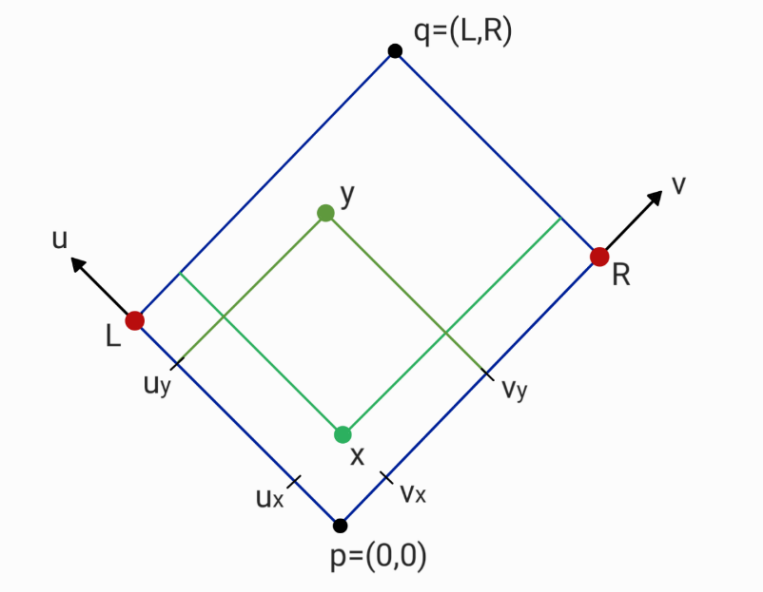

Figure 5.1: The 2D causal diamond labelled with null coordinates. The Joint is indicated by the red dots, and for some $x \prec y \in \diamond$, $\partial\mathcal{J}^+(x)$ and $\partial\mathcal{J}^-(y)$ are shown in green.

We work with null coordinates centred at point p as this best fits the symmetry of the problem. We clearly have $V_{xy} = (u_y - u_x)(v_y - v_x)$, and hence:

$$Y_\rho(x) = \int_{u_x}^{L} du_y \int_{v_x}^{R} dv_y \, e^{-\rho\,(u_y - u_x)(v_y - v_x)} \tag{5.5}$$

is the contribution of from every interval $A[x, y]$ for fixed x and,

$$X_\rho = \int_0^L du_x \int_0^R dv_x Y_\rho(x) \tag{5.6}$$

is the sum of the contributions from every $x \in \diamond$. Putting it together we have:

$$\begin{aligned}\langle S(\diamond)\rangle_{xy} &= 2\rho LR - 4\rho^2 \hat{\mathcal{O}}_2 \int_0^L du_x \int_0^R dv_x \int_{u_x}^L du_y \int_{v_x}^R dv_y \, e^{-\rho\,(u_y-u_x)(v_y-v_x)} \\ &= 2\rho LR - 4\rho^2 X_\rho\end{aligned}$$

(now turning to Mathematica)

$$= 2 - 2e^{-LR\rho}. \tag{5.7}$$

This is the flat case so $R(x) = 0$, and we indeed find the joint term is equal to 2 as expected from Conjecture 4.3.1, with the $2e^{-LR}$ term clearly going to zero as $\rho \to \infty$.

It has been noted that when calculating the action this way it is far from obvious that the value of 2 is actually coming from the joint, and it was suggested that by finding some way to perform the x and y integrals simultaneously we may be able to draw more insight from the result [48].

5.2 Fixed Intervals

A novel method for calculating X_ρ is motivated by noticing that there is a significant amount of symmetry in the calculation in Equation 5.7. Remembering that we are working in flat space, so $\sqrt{-g} = 1$, we notice the contribution to X_ρ from any given interval, $A[x, y] \in \diamond$, is dependent only by the *relative* positions of x and y. This is a form of translation invariance.

Definition 5.2.1 (Fixed Interval)**.** For some manifold $\mathcal{M} \subset \mathbb{M}^d$ with coordinate chart $\{x^\mu\}$ and some constant $c \in \mathbb{R}^d$, we define $\mathcal{W}_c \coloneqq \{\tilde{A}[x, y] \subset \mathbb{M}^d \,|\, y^\mu - x^\mu = c^\mu \text{ for } x, y \in \mathcal{M}\}$. We call $\mathcal{W}_c$ the *interval set* and c its *defining vector*. A *fixed interval* is an element $i \in \mathcal{W}_c$.

Notice that all fixed intervals of defining vector c have the same volume, $V_c \coloneqq \mathrm{Vol}([i]_c)$, where $[i]_c$ is just any representative of $\mathcal{W}_c$. We may thus decompose the set of Alexandrov intervals in $\mathcal{M}$ into sets of fixed intervals $\mathcal{W}_c$. For each value of c we also want a notion the size of $\mathcal{W}_c$.

Definition 5.2.2 (Volume of Realisation)**.** For a manifold $\mathcal{M}$, the *realisation set* on that manifold with defining vector $c \in \mathbb{R}^d$, is given by $\mathcal{Z}_c \coloneqq \{x \in \mathcal{M} \,|\, x + c \in \mathcal{M}\}$. We then define the *volume of realisation* to be, $a(c) \coloneqq \mathrm{Vol}(\mathcal{Z}_c)$. Clearly, each point $x \in \mathcal{Z}_c$ corresponds to a unique fixed interval $\tilde{A}[x, x + c] \in \mathcal{W}_c$. In this way, the volume of realisation is a measure of the number of fixed intervals of defining vector c which we can fit into $\mathcal{M}$, as shown in Figure 5.3.

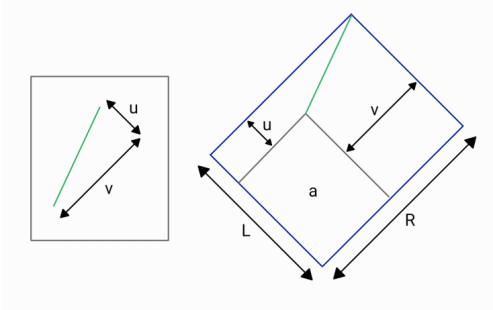

Figure 5.2: For a fixed interval of defining vector $c = (u, v)$, as shown on the left, the volume of realisation can be easily verified as $a(c) = (L - u)(R - v)$ for the diamond, as shown on the right.

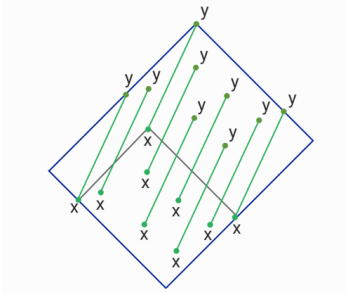

Figure 5.3: A demonstration of the ways a given fixed interval fits into the realisation set in the diamond. For any x in the realisation region, we see that the corresponding y is indeed inside the diamond.

Since all $i \in \mathcal{W}_c$ have exactly the same volume, they give exactly the same contribution to the action. The contribution from the whole of $\mathcal{W}_c$ is then just the contribution from one fixed interval multiplied by the volume of realisation.

We can hence write:

$$X_\rho = \int_{c \in \mathbb{R}^d} a(c) e^{-\rho V_c}. \tag{5.8}$$

We call this method of decomposing the integral the *weighted sum* method. We will put a subscript w on actions calculated with this method.

Diamond as a Weighted Sum

We will now show how we can calculate the action on $\diamond$ using this technique. In null coordinates, it is clear from Figure 5.1 that only fixed intervals with defining vector $c = (u, v)$ for $0 \leq u \leq L$ and $0 \leq v \leq R$ will have non-zero area of realisation. For such a vector, we can see geometrically, in Figure 5.2, that the area of realisation is given by, $a(c) = (L - u)(R - v)$. Moreover, we clearly have that $V_c = uv$. Hence, X_ρ is given by:

$$X_\rho = \int_0^L du \int_0^R dv (L - u)(R - v) e^{-\rho\, u\, v}, \tag{5.9}$$

and our action is then:

$$\begin{aligned} \langle S(\diamond) \rangle_w &= 2\rho LR - 4\rho^2 \hat{\mathcal{O}}_2 X_\rho \\ &= 2 - 2e^{-LR\rho}. \end{aligned} \tag{5.10}$$

We have recovered exactly the same result as with the standard method (Equation 5.7.

As this formulation of the problem doesn't care where any given interval is, only how often it is realised, it cannot show us that the joint contribution

actually comes from the joint as hoped. However, it can show how different *kinds* of intervals contribute to the action. By restricting the maximum size of our defining vector to some small parameters $0 < u < \epsilon$, and $0 < v < \delta$ we find that:

$$\begin{aligned}\langle S(\diamond)\rangle_{w(small)} &= 2\rho LR - 4\rho^2\hat{\mathcal{O}}_2 \int_0^\epsilon du \int_0^\delta dv (L-u)(R-v)e^{-\rho\, u\, v} \\ &= 2 - 2e^{-\delta\epsilon\rho} - 2\delta^2\epsilon^2\rho^2 e^{-\delta\epsilon\rho} - 2\delta\epsilon\rho e^{-\delta\epsilon\rho} + 2L\delta^2\epsilon\rho^2 e^{-\delta\epsilon\rho} \\ &\quad - 2LR\delta\epsilon\rho^2 e^{-\delta\epsilon\rho} + 2LR\rho e^{-\delta\epsilon\rho} + 2R\delta^2\epsilon^2\rho e^{-\delta\epsilon\rho}. \end{aligned} \tag{5.11}$$

We see that, while our subleading terms are different, we still recover the same result in the limit of $\rho \to \infty$, for fixed ϵ and δ.

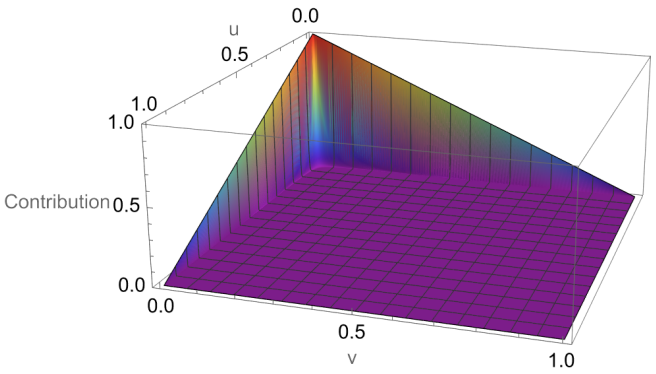

Figure 5.4: A 3D graph of the parameter space $f_\rho(u,v) = (L-u)(R-v)e^{-\rho\, u\, v}$ for fixed $\rho = 1000$. We see that the contributions come almost entirely from the null intervals (i.e. u or $v \approx 0$).

Just from inspection, it is obvious that only small intervals should contribute, and in fact we can see it explicitly by graphing the parameter space $f_\rho(u,v) = (L-u)(R-v)e^{-\rho\, u\, v}$ for fixed ρ, as shown in Figure 5.4. As $\rho \to \infty$, we clearly have that $e^{-\rho uv} \to 0$ for any non-zero volume uv. So, for large ρ, it is only as we take $uv \to 0$ that we imagine some non-zero contribution to the action might be produced. As previously discussed, elements along the (future) light cone of a given element are the 'nearest neighbours', giving intuition to why it is these kind of intervals that contribute.

It is important to note that this result is *not* the same as just considering links. While ϵ, δ can be arbitrarily small, they are still assumed to be non-zero hence big compared to the density as $\rho \to \infty$.

In fact, remembering that the different terms of $\hat{\mathcal{O}}_2$ correspond to the different types of order intervals that we are considering, we can find the contribution from just links to the action directly by just performing the calculations from Equation 5.7 or 5.10 without the $\hat{\mathcal{O}}_2$ operator. In this case we find that the action diverges as $\langle S(\diamond)\rangle_{(links)} \sim \rho$.

We will later see that this dependence only on 'small' intervals is general and can be used to simplify certain calculations where the upper bound of the vector parameter c might be complicated.

5.2.1 When can we use the weighted sum method?

The method of decomposing the set of Alexandrov intervals into sets of fixed intervals is general in flat space, and so is the definition of the realisation set and volume of realisation. However, it is not generally true that all $i \in \mathcal{W}_c$ will have the same volume.

For this reason, we have only described this method in the embedded regime. In the isolated regime, fixed intervals in a causally non-convex manifold may not have the same volume, as we may have poke-over. Hence, in the isolated regime, this method would only be applicable to causally convex manifolds, for which it is equivalent to the embedded regime.

5.2.2 How do we find the volume of realisation?

For a flat manifold $\mathcal{M}$, working in the embedded regime, we can use a method called *cloning* to find the volume of realisation. For some defining vector c, to find the realisation set $\mathcal{Z}_c$, we *clone* our manifold, and translate it by c, $\mathcal{M} - c \coloneqq \{x - c \in \mathcal{M}\}$. The realisation set is then just the intersection of our clone with $\mathcal{M}$, i.e. $\mathcal{Z}_c = (\mathcal{M} - c) \cap \mathcal{M}$. This is clearly equivalent to our original definition (5.2.2). This method is illustrated in Figures 5.5 and 5.6.

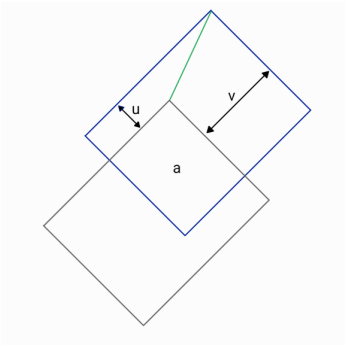

Figure 5.5: An example of using the 'cloning' method to find the volume of realisation for a causal diamond. The diamond is shown in blue and its clone is in grey. Their spatial distance from one another is the green fixed interval with defining vector $c = (u, v)$.

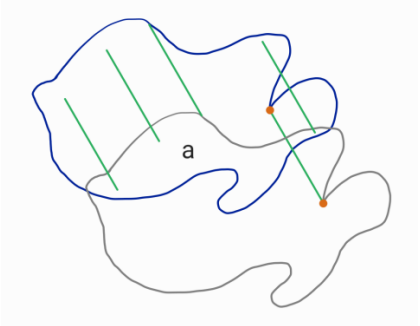

Figure 5.6: An example of the cloning method for an arbitrary manifold. The distance between the two manifolds is shown by the green line between two orange dots. Its volume of realisation is given by a.

5.3 Non-Additivity

Another important property of the action is that it is not additive. If we consider some disjoint partition of a causal set, $\mathcal{C} = \mathcal{C}_1 \cup \mathcal{C}_2$, then the action on either region individually is given by only considering when x, y are both in that region.

However, when considering the action on $\mathcal{C}$ as a whole, we must also consider order intervals between the two regions, i.e. $x \in \mathcal{C}_1, y \in \mathcal{C}_2$. Hence we have $S(\mathcal{C}) \neq S(\mathcal{C}_1) + S(\mathcal{C}_2)$ A measure of these missing contributions is given by the *mutual information* between these two regions and is defined by:

$$MI(\mathcal{C}; \mathcal{C}_1, \mathcal{C}_2) = S(\mathcal{C}) - S(\mathcal{C}_1) - S(\mathcal{C}_2). \tag{5.12}$$

We would like to define a measure of the mutual information between two manifolds, not just two causets. For this purpose, we define a *2D bilocal action*, in analogy with Equation 4.6, as:

$$S(\mathcal{C}; \mathcal{C}_1, \mathcal{C}_2) = 2N(\mathcal{C}_1, \mathcal{C}_2) - 4N_0(\mathcal{C}_1, \mathcal{C}_2) + 8N_1(\mathcal{C}_1, \mathcal{C}_2) - 4N_2(\mathcal{C}_1, \mathcal{C}_2), \tag{5.13}$$

where $N(\mathcal{C}_1, \mathcal{C}_2)$ is the number of elements in $\mathcal{C}_1$, and $N_k(\mathcal{C}_1, \mathcal{C}_2)$ is the number of order intervals, $I(x, y)$, of cardinality k, with $x \in \mathcal{C}_1$ and $y \in \mathcal{C}_2$ [46].[3]

For some disjoint union of submanifolds $\mathcal{X}, \mathcal{Y} \subset \mathcal{M}$, we can now define the *discrete bilocal action* as the random variable $\hat{\mathbf{MI}}(\mathcal{X}, \mathcal{Y})$ associated with the causal set mutual information, analogously to how we defined the discrete action from the 2D action. We will henceforth denote the expectation value of this as, $\langle MI(\mathcal{X}, \mathcal{Y}) \rangle$, and refer to it as the mutual information between the two regions.

5.3.1 The Causal Set Euler Characteristic

For an obvious example of non-additivity, we can consider taking some causal diamond and splitting it into subdiamonds.

As shown in Figure 5.7 each subdiamond is a causal diamond in its own right. We saw in Equations 5.7 and 5.10 that the action is independent on the size of the diamond. Hence each subdiamond will also give a contribution of 2 and so clearly:

$$\begin{aligned} \langle S(\diamond) \rangle &= 2 \\ &\neq \\ \sum_{i=1}^{9} \langle S(i) \rangle &= 2 \times 9 = 18. \end{aligned} \tag{5.14}$$

This is because we did not take into account the mutual information.

In fact, in [46], it was shown that for some partition of the causal diamond into subdiamonds, as $\rho \to \infty$ the mutual information between any adjacent regions was -2 and the mutual information between any non-adjacent regions was 0.

By analysing these contributions, it was proposed that by dividing any causally convex[4] manifold $\mathcal{M}$ into causal subdiamonds, the action on that region as a whole is given by:

$$\langle S(\mathcal{M}) \rangle_\infty = 2(F - E + V), \tag{5.15}$$

[3]The normalisation is off by a factor of 2 in this paper.

[4]When working in the embedded regime, we can relax this condition to simply any manifold without timelike boundaries.

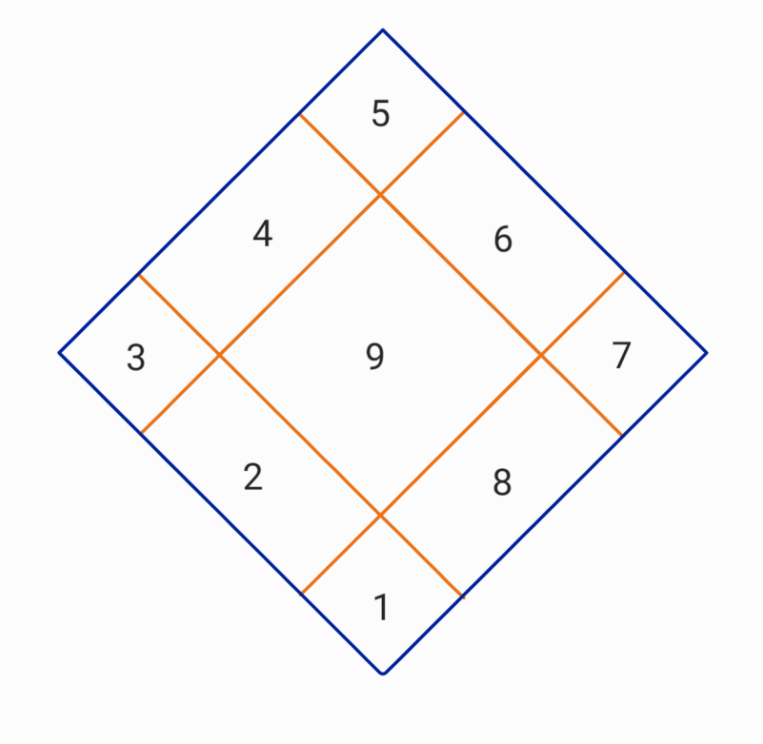

Figure 5.7: A causal diamond split into 9 subdiamonds by orange lines.

where F is the number of subdiamonds (or faces), E is the number of edges between subdiamonds, and V is the number of vertices between subdiamonds. We only include vertices which some timelike curve could traverse from one region into another. For the case shown in Figure 5.7 we have 9 faces, 12 edges, and 4 vertices so $\langle S(\mathcal{M})\rangle_\infty = 2 \times (9 - 12 + 4) = 2$ as expected.

This is strikingly similar to the Euler characteristic for a polyhedron, and we will henceforth call it the *'causal set characteristic'*. The fact that this seems to be constant (i.e. $\langle S(\mathcal{M})\rangle_\infty = 2$ for all globally hyperbolic 2D manifolds), motivates a comparison of this to the Gauss-Bonnet Theorem, although it is not believed to be related.

5.3.2 Mutual information from a Weighted Sum

It will be useful later to have some method of finding the mutual information between two regions using the weighted sum technique.

In analogy with the realisation set we define:

Definition 5.3.1 (Mutual Information Set)**.** For a manifold $\mathcal{M} = \mathcal{M}_1 \cup \mathcal{M}_2$ and a defining vector c, the *mutual information set* of for the pair of submanifolds is given by, $\mathcal{Z}_c^{MI} = \{x \in \mathcal{M}_1 \,|\, x + c \in \mathcal{M}_2\} \cup \{x \in \mathcal{M}_2 \,|\, x + c \in \mathcal{M}_1\}$.

Again, we call $a(c) = \mathrm{Vol}(\mathcal{Z}_c^{MI})$ the *volume of realisation.*

To demonstrate this, we consider a causal diamond $\diamond$ with a 'split' at $v = \frac{R}{2}$ such that it is partitioned into two regions $\diamond_1$ and $\diamond_2$.

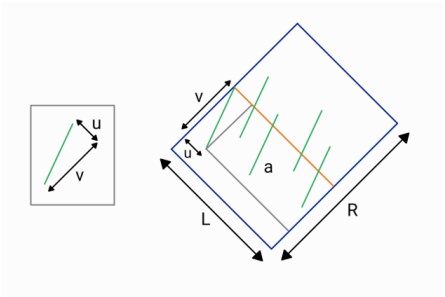

Figure 5.8: The volume of realisation for some defining vector $c = (u, v)$ where $v \leq \frac{R}{2}$. The split is shown in orange.

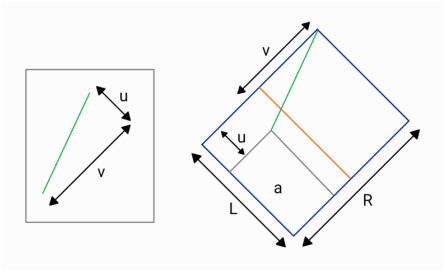

Figure 5.9: The volume of realisation for some defining vector $c = (u, v)$ where $\frac{R}{2} \leq v \leq R$. The split is shown in orange.

As we already know what the action on each of the individual regions must be, we can calculate the mutual information:

$$\begin{aligned}\langle MI(\diamond_1, \diamond_2)\rangle &= \langle S(\diamond)\rangle - \langle S(\diamond_1)\rangle - \langle S(\diamond_2)\rangle \\ &= (2 - 2e^{-LR\rho}) - (2 - 2e^{-L\frac{R}{2}\rho}) - (2 - 2e^{-L\frac{R}{2}\rho}) \\ &= -2 + 4e^{-\frac{1}{2}LR\rho} - 2e^{-LR\rho}. \end{aligned} \tag{5.16}$$

To find this directly using the weighted sum method, we must split the volumes of realisation into two cases based on parameter v of the defining vector $c = (u, v)$:

- Case 1: $0 \leq v \leq \frac{R}{2}$

$$a = (L - u)v. \tag{5.17}$$

- Case 2: $\frac{R}{2} \leq v \leq R$

$$a = (L - u)(R - v). \tag{5.18}$$

These volumes of realisation can be easily determined geometrically, as shown in Figures 5.8 and 5.9.

Our integral is then given by:

$$X_\rho = \int_0^L du \int_0^{\frac{R}{2}} dv(L - u)ve^{-\rho uv} + \int_0^L du \int_{\frac{R}{2}}^R dv(L - u)(R - v)e^{-\rho uv}, \tag{5.19}$$

and hence our mutual information is given by:

$$\begin{aligned}\langle MI(\diamond_1, \diamond_2)\rangle &= 2\rho V - 4\rho^2 X_\rho \\ &= -2 + 4e^{-\frac{1}{2}LR\rho} - 2e^{-LR\rho}, \end{aligned} \tag{5.20}$$

where there is no total volume associated with the mutual information so we take $V = 0$. We see that this method correctly reproduces the expected result from equation 5.16.

Chapter 6

Timelike Boundaries

Using the equipment so far discussed, we will now calculate the action on various regions with timelike boundaries in order to test Conjecture 4.3.2(a) and Conjecture 4.3.2(b). The simplest region to do this is the *causal rectangle*.

6.1 The Rectangle

A causal rectangle is a manifold $\square$ with two timelike boundaries (both of length T), and two (past and future) spacelike boundaries (both of length L).

Due to the timelike boundary, when trying to calculate the action with the standard method, we must split the integral into several regions depending on the relative positions of x and y. While we do not expect the length of the spacelike boundary to effect the action, it is convenient to pick $L = 2T$ as this minimises the number of integration regions we must consider.

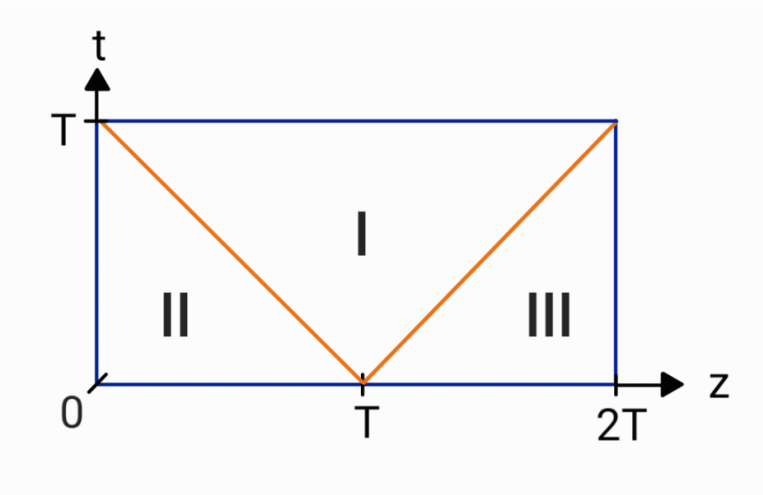

Figure 6.1: The causal rectangle is shown split integration regions of x by orange lines.

As seen in Figure 6.1, there are three regions of x we must consider: $\triangledown, \triangleleft, \triangleleft$. As we will show later, we need not consider so many regions when using the

weighted sum method. However, the weighted sum method only works in the *embedded* case, and we are interested in the contribution of timelike boundaries in both regimes. As such, it is useful to start with the standard method. We will use Cartesian coordinates (t, z) as this best reflects the symmetry of the problem. The volume V_{xy} is then given by:

$$V_{xy} = (u_y - u_x)(v_y - v_x) = \frac{1}{2} \cdot (t_y - t_x - z_y + z_x)(t_y - t_x + z_y - z_x), \tag{6.1}$$

where we used $u = \frac{1}{\sqrt{2}}(t - z)$ and $v = \frac{1}{\sqrt{2}}(t + z)$.

6.1.1 Region I

Region I is just the causal triangle $\triangledown$, shown in Figure 6.2, which is causally convex so we can calculate this without first choosing a regime.

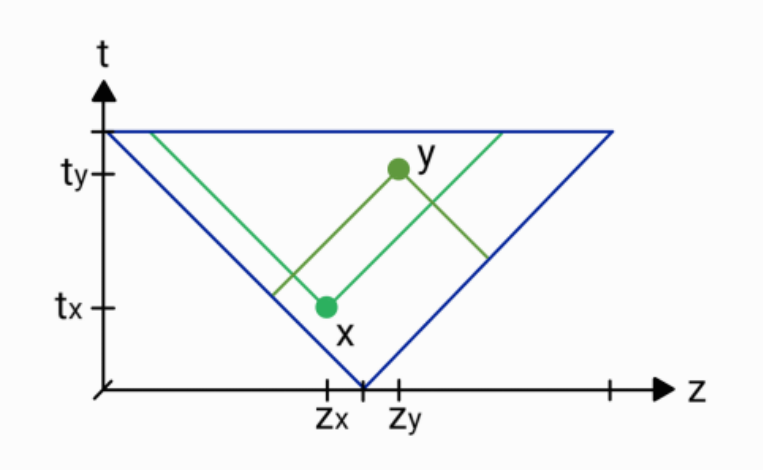

Figure 6.2: The causal triangle is shown in Cartesian coordinates. For two points $x \prec y \in \triangledown$ in the triangle, $\partial\mathcal{J}^+(x)$ and $\partial\mathcal{J}^-(y)$ are shown in green.

The action of this causal triangle is given by:

$$\begin{aligned}
\langle S(\triangledown)\rangle_{xy} &= 2\rho T^2 - 4\rho^2 \int_0^T dt_x \int_{T-t_x}^{T+t_x} dz_x \int_{t_x}^{T} dt_y \int_{z_x-(t_y-t_x)}^{z_x+(t_y-t_x)} dz_y \; \hat{\mathcal{O}}_2 e^{-\rho V_{xy}} \\
&= \frac{1}{3}\rho T^2 \left[-18\rho T^2 \, {}_2F_2\left(\frac{1}{2}, 1; \frac{3}{2}, \frac{3}{2}; -\frac{T^2\rho}{2}\right) \right. \\
&\quad +24\rho T^2 \, {}_2F_2\left(\frac{1}{2}, 1; \frac{3}{2}, \frac{5}{2}; -\frac{T^2\rho}{2}\right) - 24\rho T^2 \, {}_2F_2\left(\frac{1}{2}, 2; \frac{3}{2}, \frac{5}{2}; -\frac{T^2\rho}{2}\right) \\
&\quad -8\rho T^2 \, {}_2F_2\left(1, 1; 2, \frac{5}{2}; -\frac{T^2\rho}{2}\right) + 3\rho T^2 \, {}_2F_2\left(1, 1; \frac{5}{2}, 3; -\frac{T^2\rho}{2}\right) \\
&\quad \left. +6\left(\rho T^2 - 3\right) \, {}_2F_2\left(1, 1; \frac{3}{2}, 2; -\frac{T^2\rho}{2}\right) + 60 \right] \\
&\quad - 12\sqrt{2}\sqrt{\rho} T F\left(\frac{T\sqrt{\rho}}{\sqrt{2}}\right),
\end{aligned} \tag{6.2}$$

where $F(x)$ is the Dawson Function, and ${}_pF_q\left(a_1,...,a_p;b_1,...,b_q;x\right))$ is the generalised hypergeometric function.

This is indeed the action of the causal triangle as if we were treating it as a manifold by itself, as well as the contribution to the action of the rectangle when viewed as subregion of $\square$. This is because there are no points in the causal future of $x \in \triangledown$ that are also in $\triangleleft$ or $\triangleright$.

As the triangle is globally hyperbolic, we expect get the usual joint contribution of 2 in the infinite density limit. Indeed, taking a series expansion of ρ about infinity we see the action converges as $\langle S(\triangledown)\rangle_\infty = 2 + \frac{2}{T^2\rho} + O(\frac{1}{\rho^2})$, in line with Conjecture 4.3.1.

Weighted Sum

To consider this as a weighted sum, we parameterise our defining vector as $c = (w, h)$, where $h = t_y - t_x$ is the timelike 'height' of a fixed interval, and $w = z_y - z_x$ is the spacelike 'width'. From equation 6.1, the volume is then $V_c = V_{xy} = \frac{1}{2} \cdot (h^2 - w^2)$.

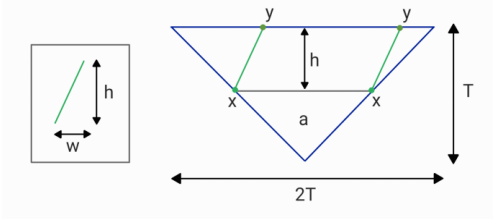

Figure 6.3: For a fixed interval of defining vector $c = (w, h)$, as shown on the left, the volume of realisation can be easily verified as $a(c) = (T - h)^2$ for the triangle, as shown on the right.

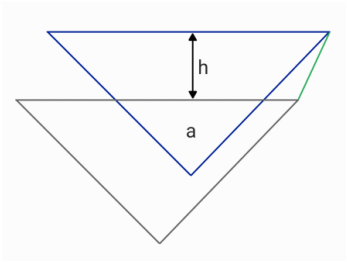

Figure 6.4: The causal triangle is shown in blue with its 'clone' shown in black. The volume of realisation is labelled a.

We see from Figures 6.3 and 6.4 that the volume of realisation is only dependent on the height of the interval, and is given by $a = (T - h)^2$.

Our mean action is then:

$$\begin{aligned}\langle S(\triangledown)\rangle_w &= 2\rho T^2 - 4\rho^2\hat{\mathcal{O}}_2 \int_0^T dh \int_{-h}^h dw\,(T-h)^2\, e^{-\rho\,\frac{1}{2}\cdot(h^2-w^2)} \\ &= 2\sqrt{2}\sqrt{\rho}tF\left(\frac{t\sqrt{\rho}}{\sqrt{2}}\right). \end{aligned} \tag{6.3}$$

We see that Mathematica provides a much more compact solution using this method and, again expanding ρ about infinity, we see the behaviour of this function in the limit is $\langle S(\triangledown)\rangle_\infty = 2 + \frac{2}{T^2\rho} + O(\frac{1}{\rho^2})$, as expected.

It is worth noting that Mathematica is unable to prove analytically that Equation 6.2 and Equation 6.3 are the same. It turns out that moving the position of the $\hat{\mathcal{O}}_2$ operator in Equation 6.2 before the integral also gives a

different solution which Mathematica also cannot show is analytically equivalent, though we know that they must be. We therefore argue that they are all the same and Mathematica is simply unable to prove it. Numerically plotting the difference between the two solutions shows that they only differ up to a very small error - which we can attribute to the inherent inaccuracies of floating point calculations - further confirming the equivalence.

6.1.2 Region II

Region II, or $\triangle$, is causally non-convex. As such, we must choose a regime. Firstly, we must note that the contributions we will calculate for region two, in either regime, will not be the same as the action $\langle S(\triangle)\rangle$. This is because we will be considering intervals with $x \in \triangle$ and $y \in \triangledown$. What we will calculate is actually $\langle S(\triangle)\rangle + \langle MI(\triangle, \triangledown)\rangle$, where $\langle MI(\triangle, \triangledown)\rangle$ is the mutual information between the two regions. We will denote our calculated quantity $\langle C(\triangle)\rangle$

Embedded Regime

When we do not have to account for poke-over, we see that we must split the y integral into two regions when using the standard method. These regions are dependent on the position of x and we call them i and ii, as shown in Figure 6.5.

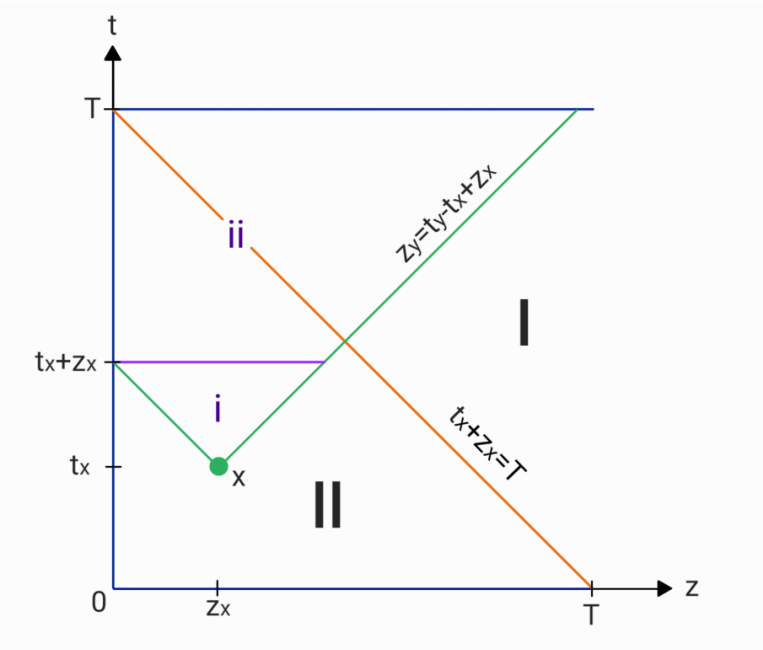

Figure 6.5: The left half of the causal rectangle is shown, with the boundary between regions I and II shown in orange. A point x in region II, along with the boundary of its causal future $\partial\mathcal{J}^+(x)$, is shown in green. The purple line partitions $\mathcal{J}^+(x)$ into regions i and ii.

Again, our interval volume is given by $V_{xy} = \frac{1}{2} \cdot (t_y - t_x - z_y + z_x)(t_y - t_x + z_y - z_x)$.
For clarity we write the y integral first:

$$\begin{aligned} Y_\rho(x) &= \int_{\mathcal{J}^+(x)} d^2y = \int_{y \in \text{i}} d^2y + \int_{y \in \text{ii}} d^2y \\ &= \int_{t_x}^{t_x+z_x} dt_y \int_{z_x-(t_y-t_x)}^{z_x+(t_y-t_x)} dz_y \, e^{-\rho V_{xy}} + \int_{t_x+z_x}^{T} dt_y \int_{0}^{z_x+(t_y-t_x)} dz_y \, e^{-\rho V_{xy}}. \end{aligned} \tag{6.4}$$

Hence, the contribution to the action from this region is given by:

$$\begin{aligned} \langle C(\triangleright) \rangle_{xy} &= 2\rho T^2 - 4\rho^2 \hat{\mathcal{O}}_2 \int_{x \in \triangleright} d^2x \int_{\mathcal{J}^+(x)} d^2y \\ &= 2\rho T^2 - 4\rho^2 \hat{\mathcal{O}}_2 \int_0^T dt_x \int_0^{T-t_x} dz_x \, Y_\rho(x) \\ &= \frac{1}{4}\sqrt{\rho} T \left(-2\sqrt{\rho} T \, {}_2F_2\left(1, 1; -\frac{1}{2}, 2; -\frac{T^2\rho}{2}\right) \right. \\ &\quad \left. -3 \, {}_2F_2\left(1, 1; \frac{1}{2}, 2; -\frac{T^2\rho}{2}\right) \right) + \sqrt{2\pi} \text{erf}\left(\frac{\sqrt{\rho}T}{\sqrt{2}}\right) - 2\sqrt{\rho} T e^{-\frac{\rho T^2}{2}}, \end{aligned} \tag{6.5}$$

where $erf(x)$ is the error function.

Expanding this result around ρ at infinity, we see this contribution diverges as:

$$\langle C(\triangleright) \rangle_\infty = -1 + \frac{1}{2}\sqrt{\frac{\pi}{2}} T \sqrt{\rho} + O(\frac{1}{\rho}). \tag{6.6}$$

Isolated Regime

For the isolated regime, we must now differentiate between regions with poke-over and regions without. As shown in Figure 6.6 we split the y integral into three regions: i, ii, and iii.

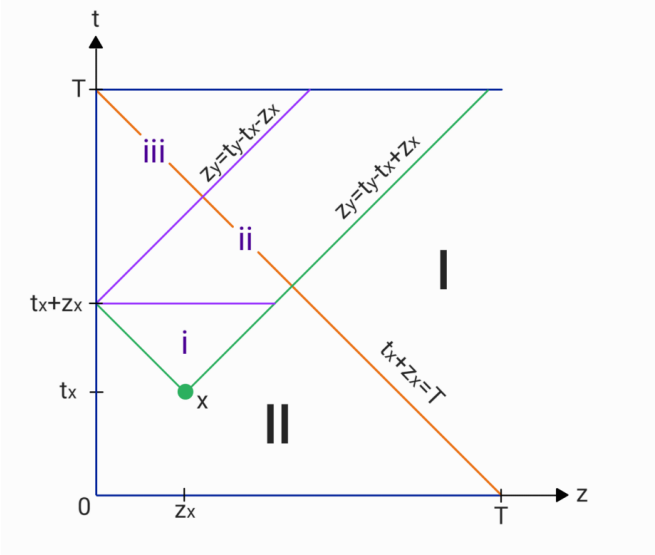

Figure 6.6: The left half of the causal rectangle is shown, with the boundary between regions I and II shown in orange. A point x in region II, along with the boundary of its causal future $\partial\mathcal{J}^+(x)$, is shown in green. The purple lines partition $\mathcal{J}^+(x)$ into regions i, ii, and iii.

For $y \in$ i or $y \in$ ii, we have that $A[x, y] \subset \square$ without having to do any extra work, and hence we can use the same volume V_{xy} as before.

However, for $y \in$ iii, there will be some volume of poke-over θ_{xy}. From Figure 6.7, we can see that this is given by $\theta_{xy} = \frac{1}{4}(t_y - z_y - t_x - z_x)^2$. The volume of the interval that is entirely inside $\square$ is just $V_{xy} - \theta_{xy}$.

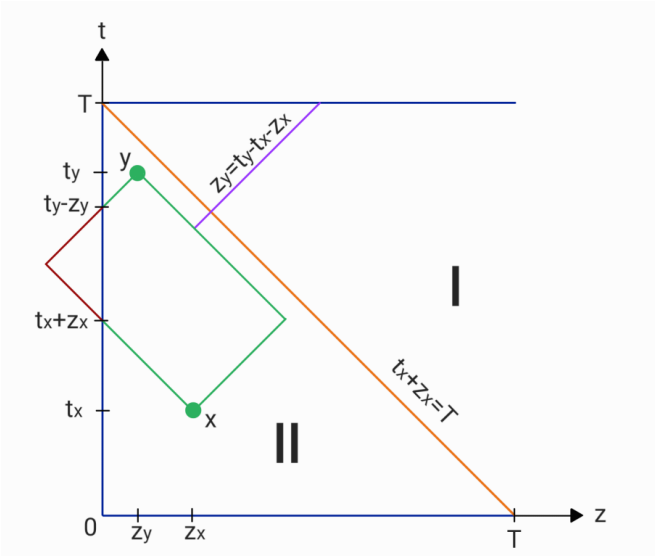

Figure 6.7: The left half of the causal rectangle is shown, with the boundary between regions I and II shown in orange. A point x in region II, and y in region iii, along with the causal interval between them, $A[x, y]$, is shown in green. The poke-over is the region shown bounded between the red line and the t-axis.

Our integral over y is then given by:

$$\begin{aligned} Y'_\rho(x) &= \int_{y\in \text{i}} d^2y + \int_{y\in \text{ii}} d^2y + \int_{y\in \text{iii}} d^2y \\ &= \int_{t_x}^{t_x+z_x} dt_y \int_{z_x-(t_y-t_x)}^{z_x+(t_y-t_x)} dz_y\, e^{-\rho\, V_{xy}} + \int_{t_x+z_x}^{T} dt_y \int_{(t_y-t_x)-z_x}^{(t_y-t_x)+z_x} dz_y e^{-\rho\, V_{xy}} \\ &\quad + \int_{t_x+z_x}^{T} dt_y \int_{0}^{(t_y-t_x-z_x)} dz_y e^{-\rho\,(V_{xy}-\theta_{xy})}. \end{aligned} \tag{6.7}$$

The contribution to the action from this region is thus:

$$\begin{aligned} \langle C'(\triangleright)\rangle_{xy} &= 2\rho T^2 - 4\rho^2 \hat{\mathcal{O}}_2 \int_{x\,\in\, \triangleright} d^2x\, Y'_\rho(x) \\ &= 2\rho T^2 - 4\rho^2 \hat{\mathcal{O}}_2 \int_0^T dt_x \int_0^{T-t_x} dz_x\, Y'_\rho(x). \end{aligned} \tag{6.8}$$

Unfortunately, Mathematica is unable to analytically calculate this expression. Splitting the integrals apart, we find that it is unable to calculate the x integral for $y \in ii$ and is not even able to do the y integral for $y \in iii$. Instead, we will use this expression to *numerically* calculate $\langle S(\square)\rangle$.

6.1.3 Putting it together

We now have an analytic result for the contribution of Region 2 in the embedded regime, and an expression which we can use for numerical integration for the isolated regime. Noticing that $\triangleright$ and $\triangleleft$ are just mirror images of each other and by symmetry must give exactly the same contribution, we have:

$$\langle S(\square)\rangle = \langle S(\triangledown)\rangle + 2\langle C(\triangleright)\rangle \tag{6.9}$$

Embedded

For the embedded case, we see that adding the analytic form of each of the contributions gives:[1]

$$\begin{aligned} \langle S(\square)\rangle = -\rho T^2 &\left({}_2F_2\left(1,1;-\frac{1}{2},2;-\frac{T^2\rho}{2}\right) - 3\,{}_2F_2\left(1,1;\frac{1}{2},2;-\frac{T^2\rho}{2}\right)\right) \\ &+ \frac{\sqrt{\rho}T\left(4F\left(\frac{T\sqrt{\rho}}{\sqrt{2}}\right) + \sqrt{\pi}\text{erf}\left(\frac{\sqrt{\rho}T}{\sqrt{2}}\right)\right)}{\sqrt{2}} + \rho T^2\left(-e^{-\frac{\rho T^2}{2}}\right). \end{aligned} \tag{6.10}$$

Expanding this result around ρ at infinity, we see that the action diverges as:

$$\langle S(\square)\rangle_\infty = T\sqrt{\frac{\pi}{2}}\sqrt{\rho} + O(\frac{1}{\rho}). \tag{6.11}$$

[1] For this calculation we used the weighted sum expression for the triangle action $\langle S(\triangledown)\rangle_w$.

This is the result predicted by Conjecture 4.3.2(a). Noticing that when we consider both left and right timelike boundaries of the rectangle, the total length of timelike boundaries is $2T$, we identify our constant from the conjecture as:[2]

$$a_0 = \frac{1}{2}\sqrt{\frac{\pi}{2}}. \tag{6.12}$$

By looking at the series expansions of each component of $\langle S(\square)\rangle$ we can identify where the contributions are coming from. We have:
$\triangledown$: A contribution of 2 from the joint.
$\triangle$: A contribution of $\frac{1}{2}\sqrt{\frac{\pi}{2}}T\sqrt{\rho}$ from the left timelike boundary of the rectangle and a contribution of -1 from the 'edge' mutual information between $\triangle$ and $\triangledown$
$\triangle$: Same as $\triangle$ but for the right timelike boundary.
In fact we can easily see that if we simply add the limits of each region we recover $\langle S(\square)\rangle_\infty = \sqrt{\frac{\pi}{2}}T\sqrt{\rho} + O(\frac{1}{\rho})$.

Isolated

For the isolated case, we go as far as we can analytically, using the integrals in Equation 6.8 that Mathematica could calculate, and the analytic form of $\langle S(\triangledown)\rangle$, then filling in the gaps with numerical integration. Fixing T and L,[3] we can plot values of ρ up to $\rho = 1000$.

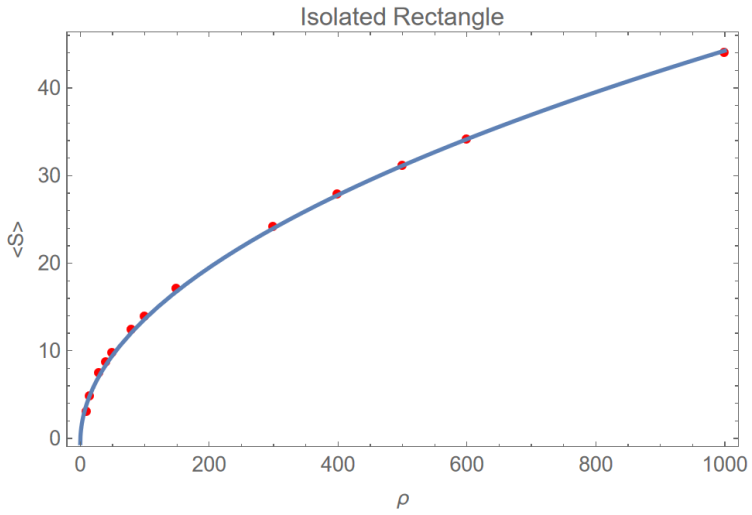

Figure 6.8: A data plot of the expected action on the rectangle with $2T = 1$ in the isolated regime, plotted in red for various values of ρ up to $\rho = 1000$. The blue line is the conjectured result $b_0(2T)\sqrt{\rho}$ where we have taken $b_0 = 0.6959$.

From the data shown in Figure 6.8, we have found the approximate value of the constant from Conjecture 4.3.2(b) as:

$$b_0 \approx 0.6959. \tag{6.13}$$

[2]This result for the case of $L = 2T$ was found by Hana Gas in her MSc project 2022: private communication by Fay Dowker.
[3]This was tested for many values of T and L.

The mean action of the rectangle in the isolated regime is then:

$$\langle S'(\square)\rangle_\infty \approx 0.6959(2T)\sqrt{\rho}. \tag{6.14}$$

6.1.4 Tall and Wide

As further evidence of the effectiveness of the weighted sum method, we now calculate the action on a rectangle of arbitrary spacelike length L and timelike height T. To do this, we must actually split the problem into two cases.

Wide Rectangle: $(L \geq T)$

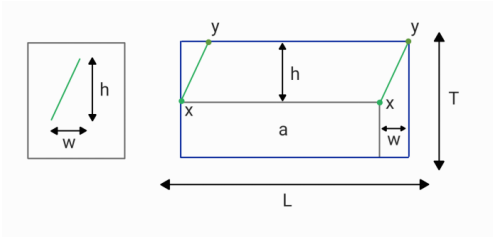

Figure 6.9: For a fixed interval of defining vector $c = (h, w)$, as shown on the left, the volume of realisation can be easily verified as $a(c) = (T-h)(L-|w|)$ for the wide causal rectangle, as shown on the right.

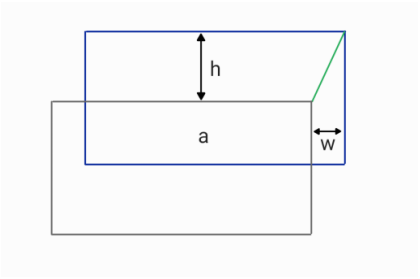

Figure 6.10: The wide causal rectangle is shown in blue with its 'clone' shown in black. The volume of realisation is labelled a.

For the wide case, as shown in Figures 6.9 and 6.10, for any fixed interval with defining vector $c = (w, h)$, it's volume of realisation is given by $a = (T-h)(L-|w|)$. The largest h such that the interval will fit somewhere in the rectangle is $h_{max} = T$, and hence the largest w we will consider when integrating w over $[-h, h]$ is $w_{max} = T \geq L$. This is important as if $w > T$ the interval would not fit in the manifold and a would be negative. Our mean action in this case is:

$$\langle S(\square)\rangle_w = 2\rho TL - 4\rho^2 \int_0^T dh \int_{-h}^{h} dw \hat{\mathcal{O}}_2 \, (T-h)(L-|w|)\, e^{-\rho \frac{1}{2}\cdot(h^2-w^2)} \tag{6.15}$$

$$= \frac{\sqrt{\rho}\left(\sqrt{\pi}T\mathrm{erf}\left(\frac{\sqrt{\rho}T}{\sqrt{2}}\right) - 2L\left(\rho T^2 - 1\right) F\left(\frac{T\sqrt{\rho}}{\sqrt{2}}\right)\right)}{\sqrt{2}}$$

$$+ \rho T\left(L - Te^{-\frac{\rho T^2}{2}}\right). \tag{6.16}$$

Tall Rectangle: $(L \leq T)$

In this case we can have $h > L$. For these values of h we cannot integrate w over $[-h, h]$, as $w > L$ is never realised in the Tall Rectangle and the associated $a(w, h)$ would be negative and thus meaningless.

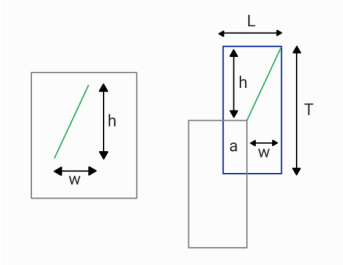

Figure 6.11: On the left, we show a fixed interval of defining vector $c = (h, w)$, for $h > L$ and $w < L$. On the right, we show the tall causal rectangle in blue, along with its clone in black. As in the wide rectangle, the volume of realisation is easily seen to be $a(c) = (T - h)(L - |w|)$.

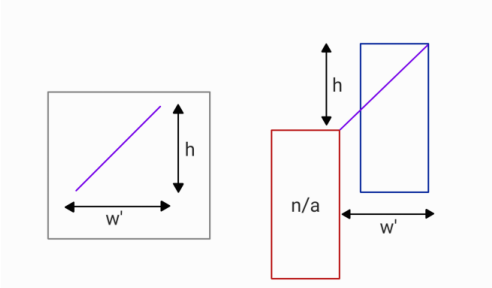

Figure 6.12: On the left, we show a fixed interval of defining vector $c = (h, w')$, for $h > L$ and $w' > L$. On the right, we show the tall causal rectangle in blue, along with its clone in red. We see that we have no volume of realisation.

As shown in Figure 6.11 and Figure 6.12, we have to split up our integral:

$$\begin{aligned}\langle S(\square)\rangle_w = 2\rho TL - 4\rho^2 \Bigg(&\int_0^L dh \int_{-h}^{h} dw \hat{\mathcal{O}}_2 \, (T-h)(L-|w|)\, e^{-\rho \frac{1}{2}\cdot(h^2-w^2)} \\ &+ \int_L^T dh \int_{-L}^{L} dw \mathcal{O}_2 \, (T-h)(L-|w|)\, e^{-\rho \frac{1}{2}\cdot(h^2-w^2)} \Bigg) \qquad (6.17) \\ = \frac{1}{2} e^{-\frac{\rho T^2}{2}} \Bigg(&\sqrt{2\pi}\sqrt{\rho} \left(T\left(L^2\rho + 1\right) \operatorname{erf}\left(\frac{L\sqrt{\rho}}{\sqrt{2}}\right) e^{\frac{1}{2}\rho\left(L^2+T^2\right)} \right. \\ &- T\left(e^{\frac{L^2\rho}{2}}\left(L^2\rho+1\right) - 1\right) e^{\frac{\rho T^2}{2}} \operatorname{erf}\left(\frac{\sqrt{\rho}T}{\sqrt{2}}\right) \\ &\left. + L\left(1-\rho T^2\right) \operatorname{erfi}\left(\frac{L\sqrt{\rho}}{\sqrt{2}}\right)\right) - 2\rho \Big(e^{\frac{L^2\rho}{2}}(L-T)(L+T) \\ &- LTe^{\frac{\rho T^2}{2}} + T^2\Big)\Bigg), \qquad (6.18)\end{aligned}$$

where $\operatorname{erfi}(x)$ is the imaginary error function.

For both the tall and the wide rectangle, expanding ρ around infinity gives: $\langle S(\square)\rangle_\infty = \langle S(\square)\rangle_\infty = \langle S(\square)\rangle_\infty = \sqrt{\frac{\pi}{2}} T\sqrt{\rho} + O(\frac{1}{\rho})$.

It is worth noting that, while the expression for $\langle S(\square)\rangle_w$ only gives the correct limiting value if we use values such that $L \leq T$, our expression for $\langle S(\square)\rangle_w$ gives us the correct limiting value even if we substitute in some $L \leq T$. This is because only 'small' intervals contribute to the action. In fact, by only considering

arbitrarily small intervals in for the wide rectangle we have:

$$\langle S(\square)\rangle_w = 2\rho T^2 - 4\rho^2 \int_0^{\epsilon} dh \int_{-h}^{h} dw \hat{\mathcal{O}}_2 \, (T-h)^2 \, e^{-\rho \frac{1}{2}\cdot(h^2-w^2)} \tag{6.19}$$

$$\begin{aligned} &= \frac{\sqrt{\rho}}{\sqrt{2}} \left(2LF\left(\frac{\epsilon\sqrt{\rho}}{\sqrt{2}}\right) \left(\rho\epsilon \left(\rho\epsilon^2(T-\epsilon) - 3T + 2\epsilon\right) + 1\right) \right. \\ &\quad \left. + \sqrt{\pi} T \mathrm{erf}\left(\frac{\sqrt{\rho}\epsilon}{\sqrt{2}}\right)\right) \\ &\quad - L\rho\left(\rho\epsilon^2(T-\epsilon) - 2T + \epsilon\right) \\ &\quad - \rho\epsilon e^{-\frac{\rho\epsilon^2}{2}} \left(-\rho T\epsilon^2 + T + \rho\epsilon^3\right). \end{aligned} \tag{6.20}$$

And we see that the in the limit the result is still $\sim \sqrt{\frac{\pi}{2}} T\sqrt{\rho} + O(\frac{1}{\rho})$.

6.1.5 Limiting Cases

Having expressions for the action when L and T are of arbitrary length immediately raises the question: What is the limiting case? Now any fixed non-zero L, T, however small, will still be large compared to the discreteness scale as we take $\rho \to \infty$. Instead, we can ask what happens when we take L or T to be the discreteness length $\rho^{-\frac{1}{2}}$. For the case that $T = \rho^{-\frac{1}{2}}$, for any density we will have that T is effectively only one element wide, and is hence equivalent to a path. We will call this construction $\mathcal{P}_{MDA}$. Taking take $\rho \to \infty$ is then just equivalent to taking the path to be infinitely long. Similarly, we call the $L = \rho^{-\frac{1}{2}}$ limiting case of the rectangle $\mathcal{A}_{MDA}$, where this is equivalent to an infinitely long antichain.

If we call an infinitely long path defined in the usual sense $\mathcal{P}$, and an antichain defined in the usual sense $\mathcal{A}$, then we can actually very easily calculate the 2D action (Equation 4.6) $S(\mathcal{P})$ and $S(\mathcal{A})$. This allows us to directly compare the how the MDA and the 2D action behave on 'the same' causal set. Note that we reinstate the factor of $\frac{1}{\hbar}$ in this subsection.

Path

For the path, each element $x \in \mathcal{P}$ will have exactly one link, one order interval of cardinality 2, and one order interval of cardinality 3 to its past. Hence:

$$\begin{aligned} R^{(2)}(x) &= (4 - 8N_0(x) + 16N_1(x) - 8N_2(x))\rho \\ &= (4 - 8\times 1 - 16\times 1 - 8\times 1)\rho \\ &= 4\rho. \end{aligned} \tag{6.21}$$

As there will be $T\sqrt{\rho}$ elements in this path, we have that:

$$\frac{1}{\hbar} S^{(2)}(\mathcal{P}) = \sum_{x\in\mathcal{P}} \frac{R^{(2)}(x)}{2} \rho^{-1} = 2T\sqrt{\rho}. \tag{6.22}$$

To compare this with the limiting case of the rectangle, we substitute $L = \rho^{-\frac{1}{2}}$ into Equation 6.16 to get:

$$\begin{aligned}\frac{1}{\hbar}\langle S(\mathcal{P}_{MDA})\rangle_\infty &= \sqrt{2e\pi}\text{erf}\left(\frac{1}{\sqrt{2}}\right)\sqrt{\rho}T - \sqrt{2e\pi}\sqrt{\rho}T + \sqrt{\frac{\pi}{2}}\sqrt{\rho}T + \sqrt{\rho}T \\ &\approx 0.942T\sqrt{\rho}. \end{aligned} \tag{6.23}$$

Antichain

$$\begin{aligned}R^{(2)}(x) &= (4 - 8N_0(x) + 16N_1(x) - 8N_2(x))\rho \\ &= (4 - 8\times 0 - 16\times 0 - 8\times 0)\rho \\ &= 4\rho. \end{aligned} \tag{6.24}$$

As there will be $T\sqrt{\rho}$ elements in this antichain, we have:

$$\frac{1}{\hbar}S^{(2)}(\mathcal{A}) = \sum_{x\in\mathcal{C}}\frac{R^{(2)}(x)}{2}\rho^{-1} = 2T\sqrt{\rho}. \tag{6.25}$$

To compare this with the limiting case of the rectangle, we substitute $T = \rho^{-\frac{1}{2}}$ into Equation 6.18 to get:

$$\begin{aligned}\frac{1}{\hbar}\langle S(\mathcal{A}_{MDA})\rangle_\infty &= \sqrt{\frac{\pi}{2}}\text{erf}\left(\frac{1}{\sqrt{2}}\right) + L\sqrt{\rho} - \frac{1}{\sqrt{e}} \\ &\approx 0.249 + L\sqrt{\rho}. \end{aligned} \tag{6.26}$$

Result

While we recover the correct form of divergence, the prefactors are extremely different and in particular for the antichain case we find the action is dependent on L which is very wrong. However, these results do not conflict with Conjecture 4.3.2(a), as the conjecture is only defined for a fixed manifold, and we have defined $\mathcal{P}_{MDA}$ and $\mathcal{A}_{MDA}$ such that their boundary lengths change with the density.

6.2 The Circle

The weighted sum method is most effective for symmetric regions, so a circular region is an obvious manifold to consider. The standard method would be extremely difficult for this manifold.

6.2.1 The Expected Result

Before we calculate the action, we will work out what we expect the result should be. This means the length of the timelike boundary of a circle must be determined.

This length is given by the proper time of a path along that boundary, which we must calculate.

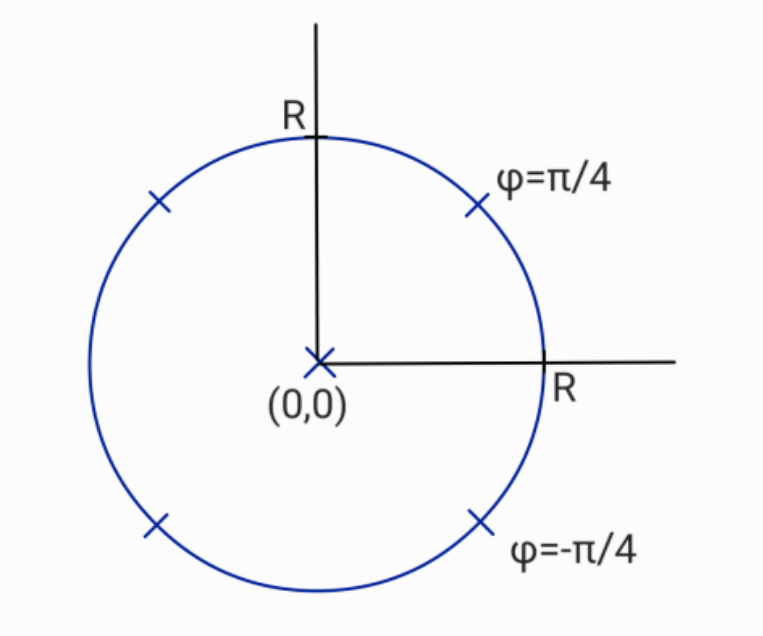

Figure 6.13: A causal circle of radius R, centred at $(0, 0$ is shown in blue. The right side of the timelike boundary is the curve between $\varphi = -\pi/4$ and $\varphi = \pi/4$.

In $\mathbb{M}^2$, our metric is given by:

$$ds^2 = -dt^2 + dz^2. \tag{6.27}$$

A circle of radius R centred at $(0, 0)$ is described by:

$$t^2 + z^2 = R^2. \tag{6.28}$$

Parameterizing with $t = R\sin(\varphi)$ and $z = R\cos(\varphi)$, our timelike boundary is represented by $\varphi \in [-\frac{\pi}{4}, \frac{\pi}{4}]$, as seen in Figure 6.13.

The proper time τ of (one side of) the boundary is then:

$$\tau = \int_{\tau_0}^{\tau_1} d\tau \tag{6.29}$$

$$= \int_{-\pi/4}^{\pi/4} d\varphi \cdot \sqrt{\left(\frac{dt}{d\varphi}\right)^2 - \left(\frac{dz}{d\varphi}\right)^2} \tag{6.30}$$

$$= R\int_{-\pi/4}^{\pi/4} d\varphi \cdot \sqrt{\cos^2(\varphi) - \sin^2(\varphi)} \tag{6.31}$$

$$= R \cdot \sqrt{\frac{2}{\pi}}\,\Gamma\left(\frac{3}{4}\right)^2 \approx R \cdot 1.198. \tag{6.32}$$

Using our value of $a_0 = \frac{1}{2}\sqrt{\frac{\pi}{2}}$ from Equation 6.12, and the fact that we must multiply our answer from Equation 6.32 by two (for each side of circle),

Conjecture 4.3.2(a) then says that the limit of the mean action should be:

$$\begin{aligned}\langle S(\circ)\rangle_\infty &= 2R\cdot\sqrt{\frac{2}{\pi}}\,\Gamma\left(\frac{3}{4}\right)^2\times\frac{1}{2}\sqrt{\frac{\pi}{2}}\times\sqrt{\rho}\\ &= R\Gamma\left(\frac{3}{4}\right)^2\sqrt{\rho}.\end{aligned}\tag{6.33}$$

6.2.2 The Calculation

To calculate the mean action on the circle, we must determine the volume of realisation. As shown in Figure 6.14 and Figure 6.15, we can use our 'cloning' technique to see that the volume of realisation is actually just given by the area of intersection between two circles of equal radii R with centers separated by Euclidean distance d.

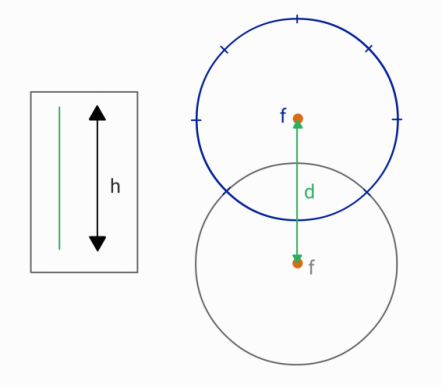

Figure 6.14: On the left, we show a fixed interval of defining vector $c = (0, h)$ of Euclidean length $d = h$. On the right, we show the causal circle in blue, along with its clone in black.

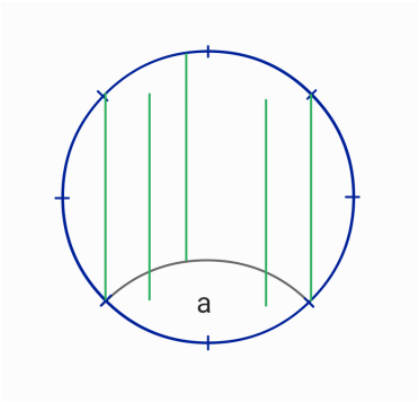

Figure 6.15: We show the causal circle in blue, with the realisation volume associated with defining vector $c = (h, 0)$ labelled by a.

This is is a solved problem [52] and is given by:

$$a(d) = 2R^2\cdot\arccos\left(\frac{d}{2R}\right) - \frac{1}{2}\cdot d\cdot\sqrt{4R^2-d^2}.\tag{6.34}$$

As seen in Figure 6.16 and Figure 6.17, we notice that this area is only dependent on the length d of the interval and not on the angle an interval makes to the t axis. This is because rotating an interval is equivalent to rotating its realisation set around the circle. Thus, due to symmetry, all realisation sets whose defining vectors c have Euclidean length d, have the same volume of realisation.

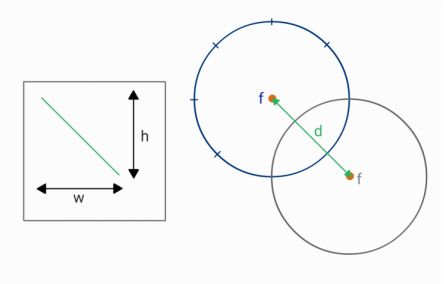

Figure 6.16: On the left, we show a fixed interval of defining vector $c = (w, h)$, of Euclidean length d. On the right, we show the causal circle in blue, along with its clone in black.

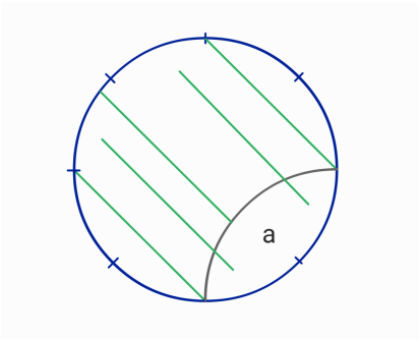

Figure 6.17: We show the causal circle in blue, with the realisation volume associated with defining vector $c = (w, h)$ labelled by a.

In Cartesian coordinates, we label our defining vectors by $c = (w, h)$ and thus have $d = \sqrt{w^2 + h^2}$. Our volume of realisation in this coordinate system is then:

$$a(w,h) = 2R^2 \cdot \arccos\left(\frac{\sqrt{h^2+w^2}}{2r}\right) - \frac{1}{2} \cdot \sqrt{h^2+w^2} \cdot \sqrt{4R^2 - h^2 - w^2}. \tag{6.35}$$

The maximum size of interval we can fit in the circle is $d_{\max} = 2R$. Remembering that $V_{xy} = \frac{1}{2}(h^2 - w^2)$, we can now calculate the mean action:

$$\langle S(\circ) \rangle_w = 2\rho \cdot \pi R^2 - 4\rho^2 \hat{\mathcal{O}}_2 \int_0^{2R} dh \int_{-h}^{h} dw\, a(w,h)\, e^{-\frac{\rho}{2}(h^2 - w^2)}. \tag{6.36}$$

Technically, we have cheated by taking these integration bounds, as for $w, h \approx R$ we have $d \approx R^2\sqrt{2}$, meaning we are considering intervals which do not fit in the circle. However, as we expect contributions from large intervals to be suppressed in the limit as $\rho \to \infty$, we argue that this will not effect the final result.

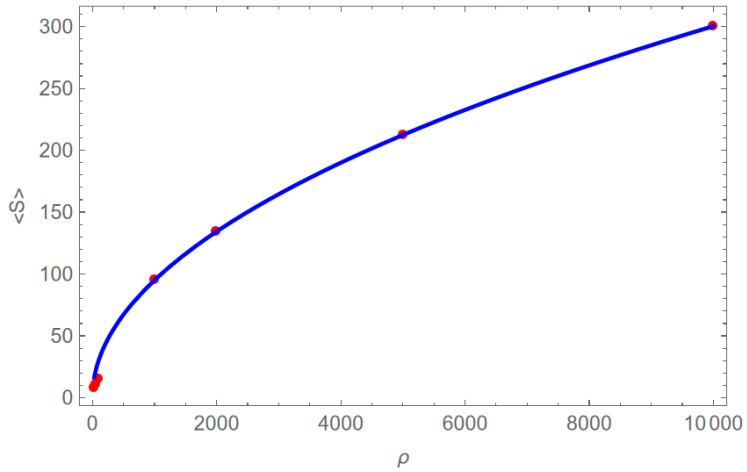

Figure 6.18: A data plot of the expected action on the rectangle with $R = 1$ in the embedded regime, plotted in red for various values of ρ up to $\rho = 10000$. The blue line is the conjectured result $\sqrt{\frac{\pi}{2}}T\sqrt{\rho}$. We see that the conjectured result is a good fit to the data.

Even with this slight approximation, Mathematica still cannot analytically compute this integral. Instead, fixing R, we can compute numerical results up to $\rho = 10000$ where, as seen in Figure 6.18 we find that it is in complete agreement with the conjectured result from Equation 6.33.

Chapter 7

Holes

As discussed in Section 3.2, we don't expect a physically meaningful spacetime to have holes. With this in mind, we will consider two manifolds. The first is the a causal rectangle with a smaller causal rectangle removed from its centre, and the second is a causal diamond with smaller causal diamond removed from its centre. We will refer to these as the *Timelike Doughnut* $\mathcal{T}_D$ and *Null Doughnut* $\mathcal{N}_D$ respectively. We will work in the *embedded* regime for most of this chapter as it makes calculations significantly simpler, but will return to discuss how these results are expected to differ from the *isolated* regime at the end of the chapter.

7.1 Embedded Regime

7.1.1 The Timelike Doughnut

To make our calculation as simple as possible, we define our Timelike Doughnut $\mathcal{T}_D$ to be as symmetric as possible, as shown in Figure 7.1.

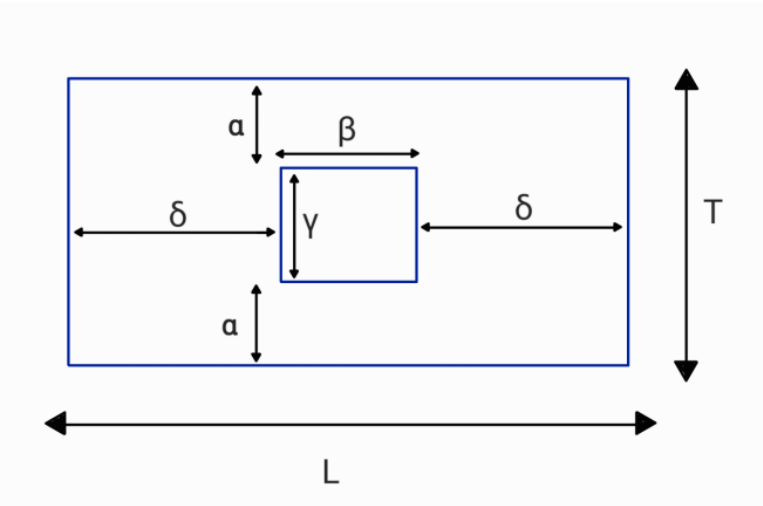

Figure 7.1: A symmetric case of the Timelike Doughnut. It is constructed such that $\alpha = \frac{T-\gamma}{2}$ and $\beta = \frac{L-\delta}{2}$.

We will call the outer rectangle (without the hole) ▭, and call the hole ▨.

It is, of course, simplest to use the weighted sum method. In fact, if we consider the problem from the perspective of mutual information, we can also further simplify it. We have:

$$\langle S(\mathcal{T}_D)\rangle = \langle S(\square)\rangle - \langle S(\blacksquare)\rangle - \langle MI(\square,\blacksquare)\rangle. \tag{7.1}$$

As we already know, the form of $\langle S(\square)\rangle$ and $\langle S(\blacksquare)\rangle$ from Chapter 6, we can determine $\langle S(\mathcal{T}_D)\rangle$ from $\langle MI(\square,\blacksquare)\rangle$ using Equation 7.1 with no more work than if we were to calculate $\langle S(\mathcal{T}_D)\rangle$ directly.

By inspection, the volumes of realisation when considering $\langle MI(\square,\blacksquare)\rangle$ appear simpler than those associated with $\langle S(\mathcal{T}_D)\rangle$, so we choose to calculate $\langle MI(\square,\blacksquare)\rangle$.

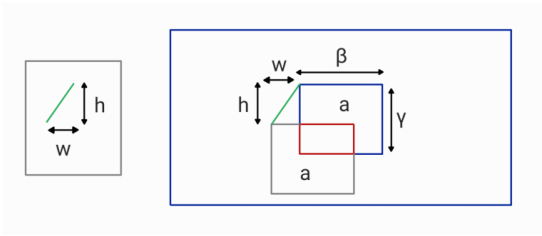

Figure 7.2: The volume of realisation for $0 \leq h \leq \frac{1}{2}(T-\gamma)$ is shown as two areas. The first is bounded between the grey boundary of the clone and the red line, and represents intervals which go from the doughnut into the hole. The second is bounded between the boundary of the hole and the red line, and represents intervals which go from the hole into the doughnut. Both these areas are equal and are labelled a.

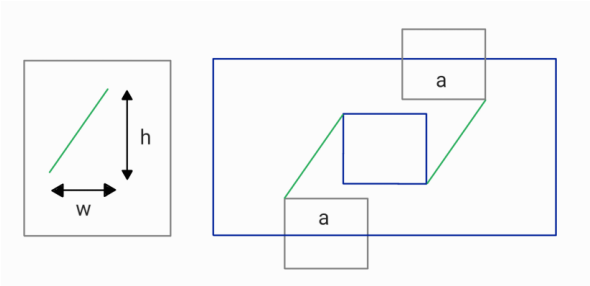

Figure 7.3: The volume of realisation for $\frac{1}{2}(T-\gamma) \leq h \leq \frac{1}{2}(T-\gamma)+\gamma$ is shown as two areas. The first is bounded between the grey boundary of the lower clone and the lower spacelike boundary of the rectangle, and represents intervals which go from the doughnut into the hole. The second is bounded between the grey boundary of the upper clone and the upper spacelike boundary of the rectangle, and represents intervals which go from the hole into the doughnut. Both these areas are equal and are labelled a.

As shown in Figure 7.2 and Figure 7.3, we must split the volumes of realisation for $\langle MI(\square,\blacksquare)\rangle$ into three cases based the height parameter of the defining vector $c = (w, h)$. The form of these volumes of realisation can be easily calculated as:

- Case 1: $0 \leq h \leq \frac{1}{2}(T-\gamma)$

$$a = 2(|w|(\gamma - h) + \beta h). \tag{7.2}$$

- Case 2: $\frac{1}{2}(T-\gamma) \leq h \leq \frac{1}{2}(T-\gamma)+\gamma$

$$a = \beta(\gamma - 2h + T). \tag{7.3}$$

- Case 3: $\frac{1}{2}(T-\gamma)+\gamma \leq h \leq T$

$$a = 0. \tag{7.4}$$

It is worth noting that for these volumes of realisation to be accurate, we must assume that the outer timelike boundaries of the rectangle are far enough away from the timelike boundaries of the hole such that no causal curves starting in the hole could reach the outer timelike boundaries.
The mutual information is then given by:

$$\begin{aligned}
\langle MI(\square, \blacksquare)\rangle &= -4\rho^2\hat{\mathcal{O}}_2\Bigg[\int_0^{\frac{1}{2}(T-\gamma)} dh \int_{-h}^{h} dw\, 2(|w|(\gamma-h)+\beta h)e^{-\rho\frac{1}{2}\cdot(h^2-w^2)} \\
&\quad + \int_{\frac{1}{2}(T-\gamma)}^{\frac{1}{2}(T-\gamma)+\gamma} dh \int_{-h}^{h} dw\, \beta(\gamma-2h+T)e^{-\rho\frac{1}{2}\cdot(h^2-w^2)}\Bigg] \\
&= -\frac{1}{8}\sqrt{\rho}\left[8\sqrt{2\pi}\gamma\mathrm{erf}\left(\frac{\sqrt{\rho}(T-\gamma)}{2\sqrt{2}}\right) + 2\beta\sqrt{\rho}(T-3\gamma)\left(\rho(T-\gamma)^2-4\right)\right. \\
&\quad + \sqrt{2}\beta\left(-\left(\rho^2(T-3\gamma)(T-\gamma)^3\right)+4\rho(T-7\gamma)(T-\gamma)+32\right)F\left(\frac{(T-\gamma)\sqrt{\rho}}{2\sqrt{2}}\right) \\
&\quad + 4\sqrt{2}\beta\left(\rho(\gamma+T)^2-4\right)F\left(\frac{(T+\gamma)\sqrt{\rho}}{2\sqrt{2}}\right) \\
&\quad \left. + \sqrt{\rho}e^{-\frac{1}{8}\rho(T-\gamma)^2}\left(8\gamma(\gamma-T)-\rho(T-3\gamma)(T-\gamma)^3\right)\right].
\end{aligned} \tag{7.5}$$

So, from Equation 7.1, we have:

$$\begin{aligned}
\langle S(\mathcal{T}_D)\rangle &= \frac{1}{8}\sqrt{\rho}\left[2\sqrt{2}\left(L\left(\gamma^2\rho-1\right)F\left(\frac{\gamma\sqrt{\rho}}{\sqrt{2}}\right)-2\sqrt{\pi}\gamma\mathrm{erf}\left(\frac{\gamma\sqrt{\rho}}{\sqrt{2}}\right)\right)\right. \\
&\quad + 4\sqrt{2}\left(\sqrt{\pi}T\mathrm{erf}\left(\frac{\sqrt{\rho}T}{\sqrt{2}}\right)-2L\left(\rho T^2-1\right)F\left(\frac{T\sqrt{\rho}}{\sqrt{2}}\right)\right) \\
&\quad + \sqrt{2}\beta\left(-\left(\rho^2(T-3\gamma)(T-\gamma)^3\right)+4\rho(T-7\gamma)(T-\gamma)+32\right)F\left(\frac{(T-\gamma)\sqrt{\rho}}{2\sqrt{2}}\right) \\
&\quad + 4\sqrt{2}\beta\left(\rho(\gamma+T)^2-4\right)F\left(\frac{(T+\gamma)\sqrt{\rho}}{2\sqrt{2}}\right) \\
&\quad + 8\sqrt{2\pi}\gamma\mathrm{erf}\left(\frac{\sqrt{\rho}(T-\gamma)}{2\sqrt{2}}\right)+2\gamma\sqrt{\rho}\left(4\gamma e^{-\frac{\gamma^2\rho}{2}}-L\right) \\
&\quad + 8\sqrt{\rho}T\left(L-Te^{-\frac{\rho T^2}{2}}\right)+2\beta\sqrt{\rho}(T-3\gamma)\left(\rho(T-\gamma)^2-4\right) \\
&\quad \left. + \sqrt{\rho}e^{-\frac{1}{8}\rho(T-\gamma)^2}\left(8\gamma(\gamma-T)-\rho(T-3\gamma)(T-\gamma)^3\right)\right].
\end{aligned} \tag{7.6}$$

Finally, by expanding around ρ at infinity we have:

$$\langle S(\mathcal{T}_D)\rangle_\infty = \sqrt{\frac{\pi}{2}}\,(T+\gamma)\,\sqrt{\rho}, \tag{7.7}$$

where we remember that $T + \gamma$ is only half of the total length of timelike boundaries.

So we see that by adding a hole with timelike boundaries to the rectangle, we just add the usual contribution of those timelike boundaries to the action. This is consistent with $a_0 = \frac{1}{2}\sqrt{\frac{\pi}{2}}$ for Conjecture 4.3.2(a).

As we expect that it is only small intervals which contribute to the boundary, the condition that no timelike curves from inside the hole can reach the boundary is unnecessary as contributions from such intervals would be negligible. In fact, by only considering arbitrarily small intervals in Case 1 of Equation 7.5, we would have also recovered the correct behaviour as $\rho \to \infty$.

We can isolate the effect of the hole more explicitly by identifying the left and right timelike boundaries of the outer rectangle, and hence turning the space around the hole into a cylinder. We call this new manifold the 'Cylindrical Doughnut' $\mathcal{C}_D$ and we call the outer cylinder $\mathcal{C}_l$.

As we defined our Timelike Doughnut such that no causal curves from inside the hole could reach the timelike boundary, the mutual information between the hole and exterior of our new Cylindrical Doughnut must be exactly the same as for the Timelike Doughnut, i.e.

$$\langle MI(\square, \boxslash) \rangle = \langle MI(\mathcal{C}_l, \boxslash) \rangle =_{\rho\to\infty} -2\sqrt{\frac{\pi}{2}}\,\gamma\,\sqrt{\rho}. \tag{7.8}$$

The causal cylinder has no timelike boundaries and no joint, and hence we have $\langle S(\mathcal{C}_l) \rangle_\infty = 0$, as shown in [48]. We also know that $\langle S(\boxslash) \rangle_\infty = \sqrt{\frac{\pi}{2}}\gamma\sqrt{\rho}$, so we therefore have that:

$$\langle S(\mathcal{C}_D) \rangle_\infty = \langle S(\mathcal{C}_l) \rangle_\infty - \langle S(\boxslash) \rangle_\infty - \langle MI(\mathcal{C}_l, \boxslash) \rangle_\infty = \sqrt{\frac{\pi}{2}}\gamma\sqrt{\rho}. \tag{7.9}$$

These results are in support of Conjecture 4.3.2(a).

If we imagine pushing the boundaries of either of our doughnuts out to infinity, then we are just left with Minkowski space with a hole in it and see that that too must have a divergent action. We argue that the adding any holes with timelike boundaries to a manifold will cause its action to diverge.

7.1.2 The Null Doughnut

The Null Doughnut $\mathcal{N}_D$ is a causal diamond with a smaller causal diamond removed from the centre. To calculate the action on the Null Doughnut, a perfectly valid approach would be to do exactly the same thing as for the Timelike Doughnut by choosing the most symmetric case, calculating the mutual information between the interior and the exterior, and perform a sum analogous to Equation 7.1. However, we notice that the Null Doughnut can also be constructed by taking a causal diamond, splitting it up into nine subdiamonds, and then removing the centre diamond.

Remembering Section 5.3.1, we actually have a shortcut for finding the limit of the action on a region partitioned into subdiamonds which accounts for all the mutual information between regions: the causal set characteristic!

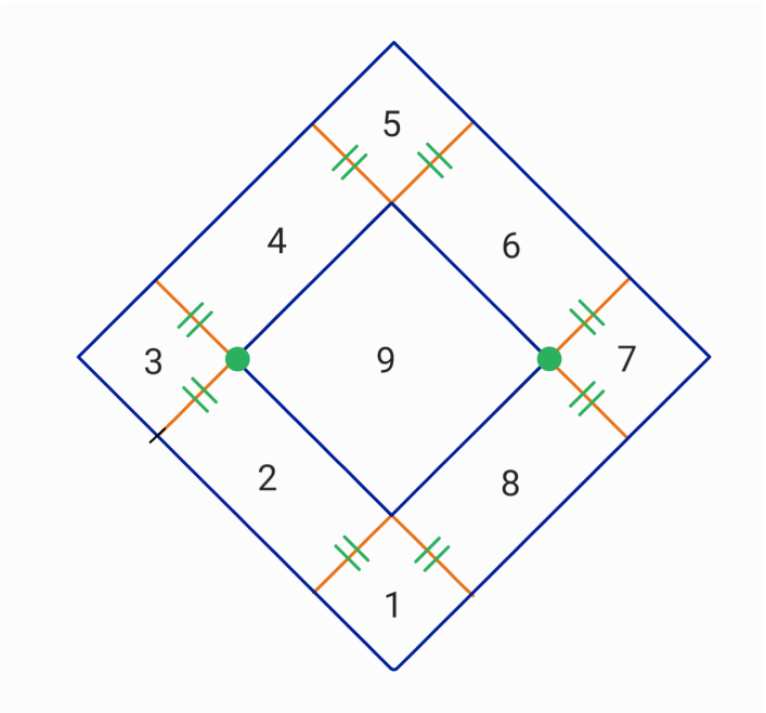

Figure 7.4: The Null Doughnut is shown partitioned by orange lines into 8 subdiamonds, where subdiamond 9 is the hole. The green dots show the vertices, and the green dashes show the edges.

As shown in shown in Figure 7.4, we do not count edges between $\mathcal{N}_D$ and the hole, and we do not count the vertices at the top and bottom of the hole, as we defined vertices to only be counted if a timelike curve can go through it. We hence have 8 faces, 8 edges, and 2 vertices.

Our causal set characteristic, and hence the action, is given by:

$$\langle S(\mathcal{N}_D)\rangle_\infty = 2 \times (8 - 8 + 2) = 4. \tag{7.10}$$

If we imagine pushing the outer boundaries of $\mathcal{N}_D$ to infinity and hence removing the outer joint term, then we argue that the consequence of adding a null hole to a space is just that we must add 2 to the action. At first glance this is somewhat of a ludicrous result, as it would mean we could add an arbitrary number of null holes of arbitrary size to a spacetime and barely change the action.

However, this is simply a result of us working in the embedded regime. While we are calculating the action on a region with a hole, we are assuming that this region is part of an underlying spacetime that is hole free.

If we truly wish to test the effect of adding a hole to a spacetime we must work in the isolated regime. However, that does not mean that these are useless results. We hope to draw insight into what form the isolated results will take by considering the embedded ones.

7.2 Isolated Regime

Working in the isolated regime poses many more problems than the embedded. Not only must we forbid poke-over - which is a difficult task in itself due to the number of regions we must consider and the difficulty Mathematica has performing the kinds of integrals involved - but we must also now be be more careful with which y are actually causally related to a given x.

For instance, as shown in Figure 7.5, in the embedded case the causal future of an x below the hole will just be the usual light cone, and can continue through the hole to the other side. This is because we are assuming there is some space for a causal curve to traverse and end up on the other side. However, in the isolated regime the causal future of x ends at the hole, as we are not assuming there is any space outside of the doughnut for a causal curve to pass through.

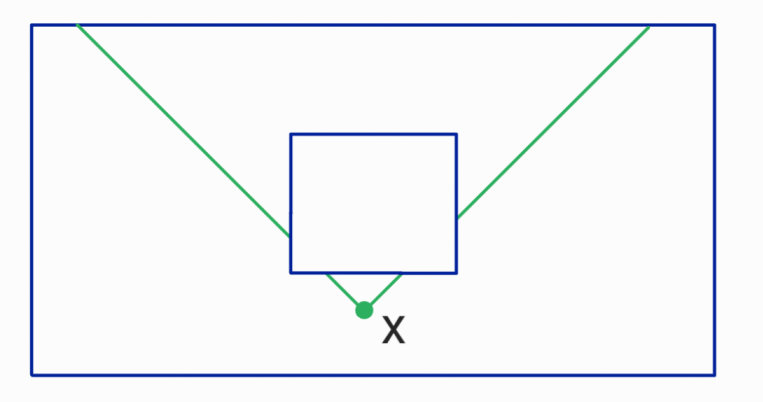

Figure 7.5: The boundary of the causal future of some x in the Timelike Doughnut is shown in green. In the embedded regime we consider it to continue to the upper spacelike boundary of the rectangle, where in the isolated regime we consider it to stop at the lower spacelike boundary of the hole.

As such, the calculations for either doughnut will require many different integration regions, with little hope that Mathematica could produce a good result.

Rather than attempt to calculate them, we will try to infer what we can from the embedded case.

Timelike Doughnut

As with the embedded case, contributions to the action come when V_{xy} is very small. For the Timelike Doughnut we see that the only way to minimise V_{xy} is to consider small intervals. As such, we argue that the contribution from the intervals which passed 'over the hole' in the embedded case (that we can no longer consider in the isolated regime) is negligible. Hence the contribution comes as usual just from the timelike boundaries.

In line with conjecture Conjecture 4.3.2(b), we expect that the action on the Timelike Doughnut in the isolated regime will be the same as Equation 7.7

in the embedded regime, but with the prefactor constant $b_0 \approx 0.6959$ replacing $a_0 = \frac{1}{2}\sqrt{\frac{\pi}{2}}$.

Null Doughnut

For the null doughnut, we again argue that the fact that we cannot consider intervals which crossed the hole to be of no significance, as the contribution from these intervals is, in general, negligible. However, in this case we there is actually another way to minimise V_{xy} other than just considering small intervals.

As seen in Figure 7.6, if we take x to be very close to the bottom right boundary of the hole and y to be very close to the top right boundary of the hole, then V_{xy} will be very small and hence we expect intervals of this form to give a contribution. We will call such intervals *squeezed intervals* as their volume is squeezed very small by the null boundaries.

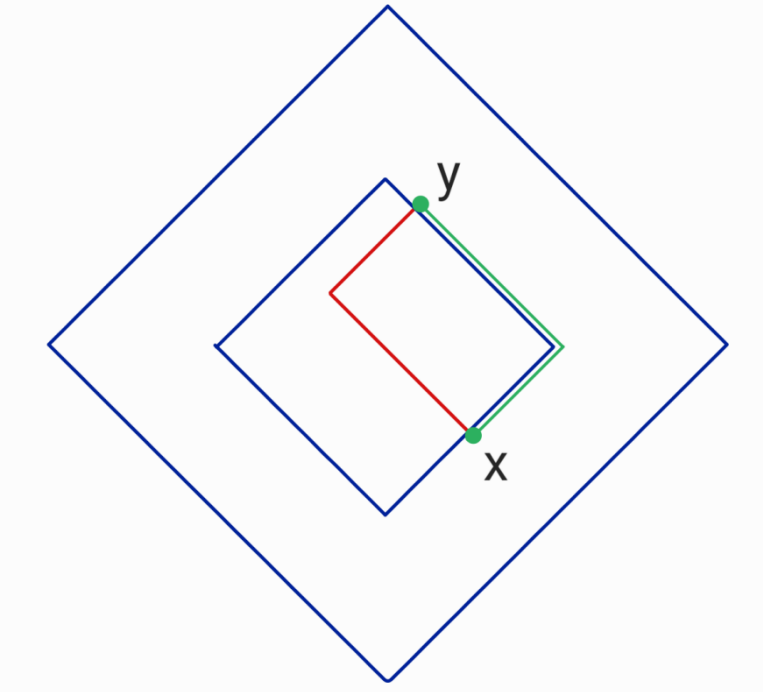

Figure 7.6: A squeezed interval near a null hole is shown. The volume between the green lines and the hole boundary V_{xy}, where the volume between the red lines and the hole boundary is the poke-over θ_{xy}. The green and red lines bound the causal interval between x and y.

In order to investigate how we expect these squeezed intervals to contribute to the action, we will consider a simple case. We can then use the result of the simple case to infer what the form of the action of the Null Doughnut - and more general causally non-convex manifolds without timelike boundaries - will be.

7.2.1 The L-Piece

The L-Piece $\mathcal{L}$ is a causally continuous, causally non-convex manifold with no timelike boundaries. From Figure 7.7 we can see that it possesses the right kind of boundaries for squeezed interval contributions to emerge. We shall calculate the action on this region.

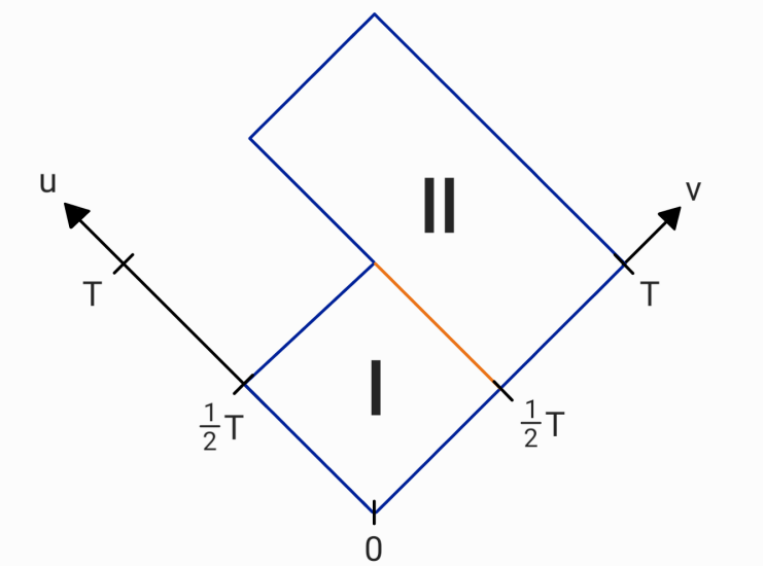

Figure 7.7: The L-Piece is shown in null coordinates. The boundary between the integration regions of x, i.e. regions I and II, is shown in orange.

As shown in Figure 7.7, we must split the integral into two regions of x which we label I and II.

Region I

As shown in Figure 7.8, given an $x \in$ I, we have two integration regions of y which we label i and ii. For $y \in$ i, there is no poke over, and we take $V_{xy}^{(i)} = V_{xy} = (u_y - u_x)(v_y - v_x)$. For $y \in$ ii, there is poke over and, as shown in Figure 7.9, the poke over volume is given by $\theta_{xy} = (\frac{T}{2} - v_x)(u_y - \frac{T}{2})$. Therefore, the volume associated to this integral is $V_{xy}^{(\text{ii})} = V_{xy} - \theta_{xy}$.

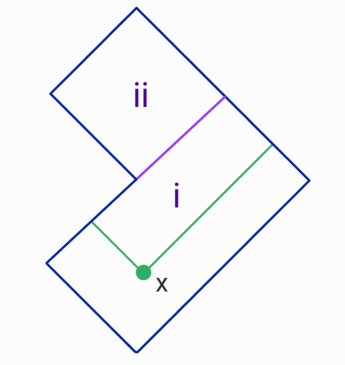

Figure 7.8: The boundary of the causal future of $x \in \mathrm{I}$ is shown in green. The purple line separates the integration regions of y, which we call i and ii.

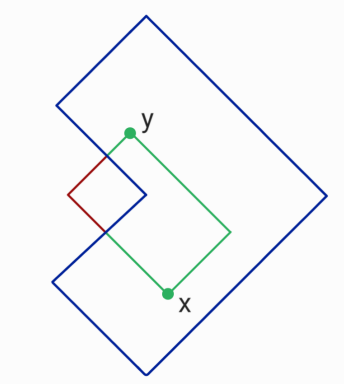

Figure 7.9: The boundary of the causal interval between $x \in \mathrm{I}$ and $y \in \mathrm{ii}$ is shown in green and red. The part bounded between the red line and the boundary of the L-Piece is the poke over region. The area of this region can be easily calculated in terms of the coordinate positions of x and y.

The y integral for $x \in \mathrm{I}$ is then given as:

$$\begin{aligned} Y_\rho^{(\mathrm{I})}(x) &= \int_{y\in \mathrm{i}} d^2y + \int_{y\in \mathrm{ii}} d^2y \\ &= \int_{u_x}^{\frac{T}{2}} du_y \int_{v_x}^{T} dv_y e^{-\rho V_{xy}} + \int_{\frac{T}{2}}^{T} du_y \int_{\frac{T}{2}}^{T} dv_y e^{-\rho(V_{xy}-\theta_{xy})}, \end{aligned} \tag{7.11}$$

and integrating over x gives us:

$$X_\rho^{(\mathrm{I})} = \int_0^{\frac{T}{2}} du_x \int_0^{\frac{T}{2}} dv_x Y_\rho^{(\mathrm{I})}(x). \tag{7.12}$$

Region II

As we can see in Figure 7.7, region II is simply a causal diamond. There is hence only one region of y which we must consider, as shown in Figure 7.10.

The integral for $x \in \mathrm{II}$ is thus given as:

$$Y_\rho^{(\mathrm{II})}(x) = \int_{u_x}^{T} du_y \int_{v_x}^{T} dv_y e^{-\rho V_{xy}} \tag{7.13}$$

and integrating over x gives us:

$$X_\rho^{(\mathrm{II})} = \int_0^{T} du_x \int_0^{\frac{T}{2}} dv_x Y_\rho^{(\mathrm{II})}. \tag{7.14}$$

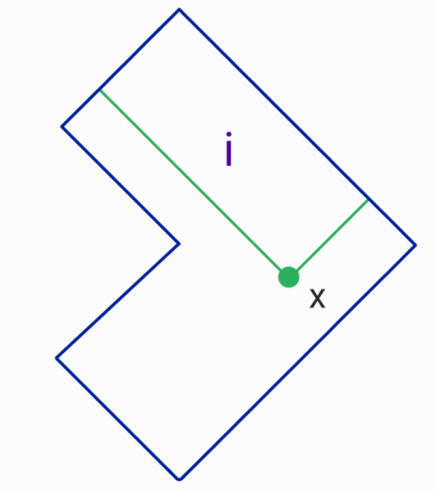

Figure 7.10: The boundary of the causal future of $x \in \text{II}$ is shown in green. We can see we just integrate y over this region as usual for a causal diamond.

Putting it together

The action on the the L piece is thus:

$$\begin{aligned}
\langle S(\mathcal{L})\rangle &= 2\rho\frac{3T^2}{4} - 4\rho^2\hat{\mathcal{O}}_2(X_\rho^{(\text{I})} + X_\rho^{(\text{II})}) \\
&= 0.5T^2\rho e^{\frac{T^2\rho}{4}}\,\text{Ei}\left(-T^2\rho\right) - T^2\rho e^{\frac{T^2\rho}{4}}\,\text{Ei}\left(-\frac{T^2\rho}{2}\right) + 0.5T^2\rho e^{\frac{T^2\rho}{4}}\,\text{Ei}\left(-\frac{T^2\rho}{4}\right) \\
&\quad + T^2\rho e^{-\frac{T^2\rho}{4}}\,\text{Ei}\left(-\frac{T^2\rho}{2}\right) - T^2\rho e^{-\frac{T^2\rho}{4}}\,\text{Ei}\left(-\frac{T^2\rho}{4}\right) - T^2\rho e^{-\frac{T^2\rho}{4}}\log(2) \\
&\quad - 2e^{\frac{T^2\rho}{4}}\,\text{Ei}\left(-T^2\rho\right) + 4e^{\frac{T^2\rho}{4}}\,\text{Ei}\left(-\frac{T^2\rho}{2}\right) - 2e^{\frac{T^2\rho}{4}}\,\text{Ei}\left(-\frac{T^2\rho}{4}\right) \\
&\quad + 4\log(T) + 2\log\left(\frac{\rho}{4}\right) - 2\,\text{Chi}\left(\frac{T^2\rho}{4}\right) + 2\,\text{Shi}\left(\frac{T^2\rho}{4}\right) + 2\gamma \\
&\quad + 2 + 4e^{-\frac{T^2\rho}{4}}\,\text{Ei}\left(-\frac{T^2\rho}{2}\right) - 4e^{-\frac{T^2\rho}{4}}\,\text{Ei}\left(-\frac{T^2\rho}{4}\right) - 4e^{-\frac{T^2\rho}{4}}\log(2) - 2e^{-\frac{3T^2\rho}{4}},
\end{aligned} \tag{7.15}$$

where $\text{Chi}(x)$ denotes the hyperbolic cosine integral, $\text{Shi}(x)$ denotes the hyperbolic sine integral and $\text{Ei}(x)$ denotes the exponential integral. Expanding this result around ρ at infinity we have:

$$\langle S(\mathcal{L})\rangle_\infty = 2\gamma + 4\log(T) - 2\log(4T^2) + 2\log(T^2\rho) = 2\gamma + \frac{1}{8}\log T^2\rho, \tag{7.16}$$

where γ is the Euler-Mascheroni constant.

Flat Trousers

This result is strikingly similar to a result calculated by Benincasa and Dowker in [46] for a causally convex region of 2D flat trousers $\mathcal{T}$. In general, Trousers is

a model spacetime used to represent a topology changing process where a single space is split into two separate pieces. This is generally seen as an undesirable spacetime and it has been shown that quantum fields behave badly on it. It was argued in [32] that this bad behaviour was due it being causally discontinuous.

Benincasa found that the action on the 2D flat trousers was given by:[1]

$$\langle S(\mathcal{T})\rangle_\infty = 8\log(\frac{\rho T^2}{4}) + 8(\gamma - 1). \tag{7.17}$$

We see exactly the same form of logarithmic divergence was found in this case, even along with the same mysterious occurrence of the Euler-Mascheroni constant.

This result is interesting, as $\mathcal{T}$ is a causally convex region, so it shows causal convexity is insufficient for a manifold to have a stable action. However, we also cannot attribute the divergence of its action to causal discontinuity. The L-Piece is causally non-convex and causally continuous, while the trousers region is causally convex but not causally continuous. As such, it appears that neither of these properties can be the cause of the logarithmic divergence.

Despite the causal convexity of the trousers, the identification of certain regions in their construction means that the trousers also have instances of squeezed intervals. In fact, the divergent region considered in [46] is visually almost identical to the L-Piece. We expect that in the case of the Null Doughnut, which also contains instances of fixed intervals, and is both causally non-convex and causally discontinuous, the action would also diverge as $\log(\rho)$.

We make the tentative conjecture that this will be the form of divergence for all non-globally hyperbolic manifolds without timelike boundaries.

[1]We get Equation 7.17 from the result in [46] accounting for the new normalisation of the action and changing to our T variable.

Chapter 8

Discussion

8.1 Summary

Causal Set Theory postulates that the key components of reality are discreteness and causality.

In Chapter 1 the need for a theory of quantum gravity and motivations for assuming that spacetime might be discrete were discussed, where we saw that, without some cut off length, many important quantities in QFT and GR can be shown to diverge.

In Chapter 2, we introduced the fundamentals of causal set theory. We gave the definition of a causal set, and gave arguments that not only can a causet completely encode the information for a spacetime, but it can do so 'approximately' uniquely. We also posed the problem that the vast majority of causal sets are non-manifold-like, then described a method for producing embeddable causal sets from a manifold, called sprinkling. We also saw that due to the lack of good analogue for a spacelike hypersurface, we must consider only the SOH formulation of QM when considering causal sets.

In Chapter 3, we introduced the dynamics of causal sets. We briefly discussed the progress towards producing a 'bottom up' model of microscopic dynamics, before focusing on an approach based on the sum over histories framework in the continuum limit. We discussed what we hope to achieve by formulating this intermediate dynamics, and how we might, from a causal set perspective, rule out many types of spacetimes which are seen in GR as physically unreasonable.

In Chapter 4, we introduced the Mean Discrete Action and various conjectures surrounding it. While the most explored case is how the action works on globally hyperbolic spacetimes, we instead took a less travelled approach in attempting to show what might go wrong if we drop this condition. We also introduced two different regimes in which we can test the action in the case that a manifold is not causally convex.

In Chapter 5, we introduced a new methodology for calculating the action on a flat manifold, giving examples in how we might use it to gain new insight about old problems. We also introduced the mutual information between two spacetime regions, and the special case of the causal set characteristic for globally

hyperbolic spacetimes. We demonstrated how the new methodology can also be applied to directly calculating the mutual information between spacetime regions.

In Chapter 6, we calculated the action on various manifolds with timelike boundaries, and in Chapter 7 we analysed how adding holes to a spacetime might cause its action to diverge. We can summarise our key, novel results as follows:

1. The action of the causal diamond is two,[1] and can be derived by considering only small intervals - shown analytically using the weighted sum method.

2. The action of the causal rectangle (of arbitrary fixed total timelike height T and spacelike length L) in the embedded regime is $\frac{1}{2}\sqrt{\frac{\pi}{2}}T\sqrt{\rho}^2$ - shown analytically using the weighted sum method.[3] In the isolated regime the action is $\approx 0.6959T\sqrt{\rho}$.

3. The action on the limiting case of the causal rectangle in the embedded regime, as we take L or T to the discreteness length and hence approximate a path or antichain respectively, do not give the correct form of the divergence as if we calculated using the 2D Action.

4. The action of the a causal circle of fixed radius is given by $\frac{1}{2}\sqrt{\frac{\pi}{2}}T\sqrt{\rho}$, where T is the total length of its timelike boundaries - shown numerically in the embedded regime.

5. The action of the Timelike Doughnut is $\frac{1}{2}\sqrt{\frac{\pi}{2}}(T+\gamma)\sqrt{\rho}$, where T is the total timelike height of the outer boundaries and γ is the total timelike height of the boundaries of the hole - shown analytically in the embedded regime.

6. The action of the Null Doughnut is four - shown using the Causal Set Euler characteristic in the embedded regime.

7. The action of the L-Piece is of the form $\sim \log(T^2\rho)$, where T is the Null length of (one side of) the equal sided diamond.

Lets now address the implications of these results.

8.2 Discussion

It was suggested in [48] that we could better identify the true origin of the joint contribution by simultaneously integrating over x and y, without choosing the standard or reverse order of integration. While we have successfully produced such a formulation in our weighted sum technique, this unfortunately has not made the origin of the joint term any clearer. While we want to show that it

[1] Finding the action on the diamond to be 2 is not a novel result, but the methodology and evidence that it works for small intervals is.

[2] This was previously shown only for $L = 2T$.

[3] Again we stress that 'total timelike height' includes both sides of the boundary.

is only intervals near the joint which produce the result, when we look at the problem in terms of volumes of realisation it appears that the contribution from any small interval must come from *everywhere* in the manifold, and we have hence not isolated the joint term.

Our results for manifolds with timelike boundaries provide strong support for Conjecture 4.3.2(a) and Conjecture 4.3.2(b). We have seen for various manifolds in the embedded regime that the action is proportional to the total timelike length of its boundary, even when the boundary is curved as for the circle. It was confirmed that the prefactor in this case is $a_0 = \frac{1}{2}\sqrt{\frac{\pi}{2}}$. We also saw that for the rectangle, moving to the isolated regime only changes the prefactor constant, which we found to be approximately 0.6959. We provided an argument that this will be the same for other manifolds with timelike boundaries in this regime. This is an especially important result as we expect the isolated regime to be a truer test of the effects of adding boundaries.

From the point of view of stationary phase heuristics, these results provide a strong indication that any spacetime with timelike boundaries will be suppressed in the path integral. We are in fact interested not in a continuum limit, but a continuum approximation, and hence in our final theory we do not expect ρ to be infinite but just very large. For any region with timelike boundaries, we then see that its action will be very large and thus the variance between sprinklings will cause their contributions to the path integral to cancel each other out. In a similar vein, we have shown that adding a hole with timelike boundaries to a space also causes the action to blow up. While this was only analytically shown for the embedded regime, analysis of the type of contributions we get to the action in this case gives a strong argument that the same will be true in the isolated regime. This is an inkling of an answer to the question of why we don't see holes in spacetime, despite them being valid solutions to the EFEs.

For non-globally hyperbolic regions without timelike boundary - such as the flat trousers, L-piece, and null doughnut - we saw that in the isolated regime, they all diverge logarithmically. We do not have a conjecture associated to this, or even an idea of what shared property of these spacetimes causes this divergence from a GR perspective (beyond failure to be globally hyperbolic). We propose that the presence of 'squeezed intervals' is the cause of this divergence. Supposing this form of logarithmic divergence survives into four dimensions, where we expect our discreteness scale to be on the order of the Planck length, we would then see that plugging in the Planck density, $\rho = l_P^{-4}$, as our discreteness scale gives us $\log(\rho) \approx 320$.

While this is clearly large compared to the result of $S = 2$ for globally hyperbolic spacetimes, it is very small compared to the value of $\sqrt{\rho} \sim 10^{69}$ for regions with timelike boundaries. We could argue that these spacetimes are therefore 'less suppressed' in the path integral.

The interpretation of 'squeezed intervals' is an interesting question in itself. They represent two causally related spacetime points which can only be connected by a null curve. Generally, for two points in a causal set there will be many different 'paths' of order relations to connect the points together, where for

this squeezed interval we could interpret V_{xy} being so small as the points being connected by only one link. It is tempting to associate some form of entropy with this idea, where the fewer paths that connect two distant points, the less favourable the configuration is. However, this argument is entirely heuristic and, as we saw with the limiting case of the rectangle, finding a correspondence between our action in the continuum limit and the behaviour of elements on the fundamental level is not straight forward.

On the topic of entropy, there is an extremely speculative, but very interesting connection between the joint term and the entropy of a black hole. If we consider our case of the embedded null doughnut - where we pushed our outer boundaries out to infinity, leaving only an empty flat space with a null hole in - then we find that the contribution from this hole to the overall action is 2. In the 4D case, our joint term is more general and is actually given by the area of a 2-sphere. So, our result would be that in a universe where we count all intervals except those that intersect a region bounded by a null hypersurface, the action is given by the area of a 2-sphere. This is strikingly similar to the entropy formula of a black hole.

The study of black hole entropy from a causal set perspective has had past success and is an active area of research. It has been shown that in two dimensions, the entropy of the black hole can be calculated by counting links which cross over the horizon [53]. Moreover, in an alternative definition of entropy (via spacetime mutual information between two regions of a causal diamond truncated by a causal horizon), it was recently shown that the entropy limited to the area of intersection between the boundaries of the causal diamond and the horizon [54].

However, tempting as this interpretation of the joint term may be, the argument is entirely heuristic and as yet we do not know how the action and entropy might be related. In fact, we do not as of yet understand what the effect of adding this extra term to the gravitational action is at all.

8.3 Going Forward

There is much work to be done moving forward. A useful and likely relatively easy task would be to extend the calculation on the flat causal rectangle to four dimensions using the weighted sum method. While the usefulness of this method is restricted to flat manifolds in the embedded regime, extending it to results in higher dimensions should be generally simple.

While this dissertation has focused more on the testing how the action works on non-globally hyperbolic spacetimes than providing evidence for Conjecture 4.3.1 there is still much more work to be done in the latter case. Specifically, showing that the conjecture holds for arbitrary curvature with no caveats would give much more weight to the assertion that the MDA truly limits to the Einstein Hilbert action. If it turns out to be true, then this would be an important step to overcoming the entropic domination of non-manifold-like causal sets.

As we defined our action with the continuum limit of a manifold of certain dimension in mind, it is only causal sets corresponding to these manifolds in

which non-local effects cancel out and we recover a local action. For a general non-manifold-like causal set of cardinality N, it has been shown that the action is of order N^2, and would hence be suppressed in the path integral [48].

However, the very fact that we have to manually pick the dimension of the manifold, rather than it emerging it naturally, indicates that our continuum regime is not the final story. This problem is natural to us having taken a top down approach, where the action was designed to reproduce the Einstein Hilbert action. For a final theory we hope the answer lies in Quantum Sequential Growth.

We stress that to justify our stationary phase heuristics further, we also need a better understanding of how these path integrals actually behave. The introduction of the discrete action means that such work has now been able to begin, and has been used to find evidence of phase transitions in causal sets [55][56].

While we focused on finding the mean of the action over sprinklings, another direction to take is to explicitly investigate its variance. This would help provide more weight to the idea of contributions cancelling out in the path integral.

If our conjectures and heuristic arguments prove true, then we would finally have an answer to why we don't observe holes or 'physically unreasonable' spacetimes.

Bibliography

[1] Cliff P. Burgess. "Quantum Gravity in Everyday Life: General Relativity as an Effective Field Theory". In: *Living Reviews in Relativity* 7.1 (Apr. 2004). DOI: 10.12942/lrr-2004-5. URL: https://doi.org/10.12942%2Flrr-2004-5.

[2] Fay Dowker. "The birth of spacetime atoms as the passage of time". In: *Annals of the New York Academy of Sciences* 1326.1 (Sept. 2014), pp. 18–25. DOI: 10.1111/nyas.12542. URL: https://doi.org/10.1111%2Fnyas.12542.

[3] Rafael D. Sorkin. "Forks in the road, on the way to quantum gravity". In: *International Journal of Theoretical Physics* 36.12 (Dec. 1997), pp. 2759–2781. DOI: 10.1007/bf02435709. URL: https://doi.org/10.1007%2Fbf02435709.

[4] Tony Rothman and Stephen Boughn. "Can Gravitons be Detected?" In: *Foundations of Physics* 36.12 (Nov. 2006), pp. 1801–1825. DOI: 10.1007/s10701-006-9081-9. URL: https://doi.org/10.1007%2Fs10701-006-9081-9.

[5] Sunil Mukhi. "String theory: a perspective over the last 25 years". In: *Classical and Quantum Gravity* 28.15 (June 2011), p. 153001. DOI: 10.1088/0264-9381/28/15/153001. URL: https://doi.org/10.1088%2F0264-9381%2F28%2F15%2F153001.

[6] Abhay Ashtekar and Eugenio Bianchi. "A short review of loop quantum gravity". In: *Reports on Progress in Physics* 84.4 (Mar. 2021), p. 042001. DOI: 10.1088/1361-6633/abed91. URL: https://doi.org/10.1088%2F1361-6633%2Fabed91.

[7] Fay Dowker. "Introduction to causal sets and their phenomenology". In: *General Relativity and Gravitation* 45.9 (Sept. 2013). DOI: 10.1007/s10714-013-1569-y. URL: https://doi.org/10.1007/s10714-013-1569-y.

[8] Rafael D. Sorkin. *1983 paper on entanglement entropy: "On the Entropy of the Vacuum outside a Horizon"*. 2014. arXiv: 1402.3589 [gr-qc].

[9] Luca Bombelli et al. "Space-time as a causal set". In: *Phys. Rev. Lett.* 59 (5 Aug. 1987), pp. 521–524. DOI: 10.1103/PhysRevLett.59.521. URL: https://link.aps.org/doi/10.1103/PhysRevLett.59.521.

[10] Rafael D. Sorkin. "First Steps with Causal Sets". In: 1991. URL: https://api.semanticscholar.org/CorpusID:117054593.

[11] S. W. Hawking, A. R. King, and P. J. Mccarthy. "A New Topology for Curved Space-Time Which Incorporates the Causal, Differential, and Conformal Structures". In: *J. Math. Phys.* 17 (1976), pp. 174–181. DOI: 10.1063/1.522874.

[12] David B. Malament. "The class of continuous timelike curves determines the topology of spacetime". In: *Journal of Mathematical Physics* 18 (1977), pp. 1399–1404. URL: https://api.semanticscholar.org/CorpusID:121083808.

[13] AV0637 Levichev. "Prescribing the conformal geometry of a Lorentz manifold by means of its causal structure". In: *Soviet Math. Dokl.* Vol. 35. 452-455. 1987, p. 133.

[14] Onkar Parrikar and Sumati Surya. "Causal topology in future and past distinguishing spacetimes". In: *Classical and Quantum Gravity* 28.15 (July 2011), p. 155020. DOI: 10.1088/0264-9381/28/15/155020. URL: https://doi.org/10.1088%2F0264-9381%2F28%2F15%2F155020.

[15] Luca Bombelli. "Statistical Lorentzian geometry and the closeness of Lorentzian manifolds". In: *Journal of Mathematical Physics* 41.10 (Oct. 2000), pp. 6944–6958. DOI: 10.1063/1.1288494. URL: https://doi.org/10.1063%2F1.1288494.

[16] David A. Meyer. "The dimension of causal sets". In: 1988. URL: https://api.semanticscholar.org/CorpusID:116953835.

[17] David A. Meyer. "Spherical containment and the Minkowski dimension of partial orders". In: *Order* 10 (1993), pp. 227–237. URL: https://api.semanticscholar.org/CorpusID:122879180.

[18] Graham Brightwell and Ruth Gregory. "Structure of random discrete spacetime". In: *Phys. Rev. Lett.* 66 (3 Jan. 1991), pp. 260–263. DOI: 10.1103/PhysRevLett.66.260. URL: https://link.aps.org/doi/10.1103/PhysRevLett.66.260.

[19] David Rideout and Petros Wallden. "Spacelike distance from discrete causal order". In: *Classical and Quantum Gravity* 26.15 (July 2009), p. 155013. DOI: 10.1088/0264-9381/26/15/155013. URL: https://doi.org/10.1088%2F0264-9381%2F26%2F15%2F155013.

[20] Seth Major, David Rideout, and Sumati Surya. "Stable homology as an indicator of manifoldlikeness in causal set theory". In: *Classical and Quantum Gravity* 26.17 (Aug. 2009), p. 175008. DOI: 10.1088/0264-9381/26/17/175008. URL: https://doi.org/10.1088%2F0264-9381%2F26%2F17%2F175008.

[21] Dionigi M. T. Benincasa and Fay Dowker. "Scalar Curvature of a Causal Set". In: *Physical Review Letters* 104.18 (May 2010). DOI: 10.1103/physrevlett.104.181301. URL: https://doi.org/10.1103%2Fphysrevlett.104.181301.

[22] Daniel J. Kleitman and Bruce Rothschild. "Asymptotic enumeration of partial orders on a finite set". In: *Transactions of the American Mathematical Society* 205 (1975), pp. 205–220. URL: https://api.semanticscholar.org/CorpusID:122064712.

[23] FAY DOWKER, JOE HENSON, and RAFAEL D. SORKIN. "QUANTUM GRAVITY PHENOMENOLOGY, LORENTZ INVARIANCE AND DISCRETENESS". In: *Modern Physics Letters A* 19.24 (Aug. 2004), pp. 1829–1840. DOI: 10.1142/s0217732304015026. URL: https://doi.org/10.1142%2Fs0217732304015026.

[24] Sumati Surya. "The causal set approach to quantum gravity". In: *Living Reviews in Relativity* 22.1 (Sept. 2019). DOI: 10.1007/s41114-019-0023-1. URL: https://doi.org/10.1007%2Fs41114-019-0023-1.

[25] Seth A Major, David Rideout, and Sumati Surya. "Spatial hypersurfaces in causal set cosmology". In: *Classical and Quantum Gravity* 23.14 (July 2006), pp. 4743–4751. DOI: 10.1088/0264-9381/23/14/011. URL: https://doi.org/10.1088%2F0264-9381%2F23%2F14%2F011.

[26] RAFAEL D. SORKIN. "QUANTUM MECHANICS AS QUANTUM MEASURE THEORY". In: *Modern Physics Letters A* 09.33 (Oct. 1994), pp. 3119–3127. DOI: 10.1142/s021773239400294x. URL: https://doi.org/10.1142%2Fs021773239400294x.

[27] Fay Dowker. *Causal sets and the deep structure of spacetime*. 2005. arXiv: gr-qc/0508109 [gr-qc].

[28] D. P. Rideout and R. D. Sorkin. "Classical sequential growth dynamics for causal sets". In: *Physical Review D* 61.2 (Dec. 1999). DOI: 10.1103/physrevd.61.024002. URL: https://doi.org/10.1103%2Fphysrevd.61.024002.

[29] Joe Henson. *The causal set approach to quantum gravity*. 2006. arXiv: gr-qc/0601121 [gr-qc].

[30] Petros Wallden. "Causal Sets Dynamics: Review amp; Outlook". In: *Journal of Physics: Conference Series* 453.1 (Aug. 2013), p. 012023. DOI: 10.1088/1742-6596/453/1/012023. URL: https://dx.doi.org/10.1088/1742-6596/453/1/012023.

[31] Graham Brightwell et al. ""Observables" in causal set cosmology". In: *Physical Review D* 67.8 (Apr. 2003). DOI: 10.1103/physrevd.67.084031. URL: https://doi.org/10.1103%2Fphysrevd.67.084031.

[32] Fay Dowker. *Topology change in quantum gravity*. 2002. arXiv: gr-qc/0206020 [gr-qc].

[33] Maqbool Ahmed and David Rideout. "Indications of de Sitter spacetime from classical sequential growth dynamics of causal sets". In: *Physical Review D* 81.8 (Apr. 2010). DOI: 10.1103/physrevd.81.083528. URL: https://doi.org/10.1103%2Fphysrevd.81.083528.

[34] L Smolin. "Did the Universe evolve?" In: *Classical and Quantum Gravity* 9.1 (Jan. 1992), p. 173. DOI: 10.1088/0264-9381/9/1/016. URL: https://dx.doi.org/10.1088/0264-9381/9/1/016.

[35] Stephen William Hawking. "The path-integral approach to quantum gravity". In: 1993. URL: https://api.semanticscholar.org/CorpusID:118268082.

[36] Richard P. Feynman, Robert B. Leighton, and Matthew Sands. *The Feynman Lectures on Physics, Vol. II.* Chapter 19: The principle of least action. Accessed: [21 September 2023]. 1964. URL: https://www.feynmanlectures.caltech.edu/II_19.html.

[37] S P Loomis and S Carlip. "Suppression of non-manifold-like sets in the causal set path integral". In: *Classical and Quantum Gravity* 35.2 (Dec. 2017), p. 024002. DOI: 10.1088/1361-6382/aa980b. URL: https://doi.org/10.1088%2F1361-6382%2Faa980b.

[38] John Byron Manchak. "What Is a Physically Reasonable Space-Time?" In: *Philosophy of Science* 78.3 (2011), pp. 410–420. DOI: 10.1086/660301.

[39] Stephen William Hawking and Rainer K. Sachs. "Causally continuous spacetimes". In: *Communications in Mathematical Physics* 35 (1974), pp. 287–296. URL: https://api.semanticscholar.org/CorpusID:121866829.

[40] Fay Dowker. "Introduction to causal sets and their phenomenology". In: *General Relativity and Gravitation* 45 (Sept. 2013). DOI: 10.1007/s10714-013-1569-y.

[41] Rafael D. Sorkin. *Does Locality Fail at Intermediate Length-Scales*. 2007. arXiv: gr-qc/0703099 [gr-qc].

[42] Joe Henson. "Discovering the Discrete Universe". In: *arXiv: General Relativity and Quantum Cosmology* (2010). URL: https://api.semanticscholar.org/CorpusID:118621815.

[43] Fay Dowker and Lisa Glaser. "Causal set d'Alembertians for various dimensions". In: *Classical and Quantum Gravity* 30.19 (Sept. 2013), p. 195016. DOI: 10.1088/0264-9381/30/19/195016. URL: https://doi.org/10.1088%2F0264-9381%2F30%2F19%2F195016.

[44] Benincasa DMT. "The action of a casual set". PhD thesis. Imperial College London, 2013.

[45] Alessio Belenchia, Dionigi M T Benincasa, and Fay Dowker. "The continuum limit of a 4-dimensional causal set scalar d'Alembertian". In: *Classical and Quantum Gravity* 33.24 (Dec. 2016), p. 245018. DOI: 10.1088/0264-9381/33/24/245018. URL: https://doi.org/10.1088%2F0264-9381%2F33%2F24%2F245018.

[46] Dionigi M T Benincasa, Fay Dowker, and Bernhard Schmitzer. "The random discrete action for two-dimensional spacetime". In: *Classical and Quantum Gravity* 28.10 (Apr. 2011), p. 105018. DOI: 10.1088/0264-9381/28/10/105018. URL: https://doi.org/10.1088%2F0264-9381%2F28%2F10%2F105018.

[47] Michel Buck et al. "Boundary terms for causal sets". In: *Classical and Quantum Gravity* 32.20 (Sept. 2015), p. 205004. DOI: 10.1088/0264-9381/32/20/205004. URL: https://doi.org/10.1088%2F0264-9381%2F32%2F20%2F205004.

[48] Fay Dowker. *Boundary contributions in the causal set action*. 2020. arXiv: 2007.13206 [gr-qc].

[49] Ludovico Machet and Jinzhao Wang. "On the continuum limit of Benincasa–Dowker–Glaser causal set action". In: *Classical and Quantum Gravity* 38.1 (Dec. 2020), p. 015010. DOI: 10.1088/1361-6382/abc274. URL: https://doi.org/10.1088%2F1361-6382%2Fabc274.

[50] G. W. Gibbons and S. W. Hawking. "Action integrals and partition functions in quantum gravity". In: *Phys. Rev. D* 15 (10 May 1977), pp. 2752–2756. DOI: 10.1103/PhysRevD.15.2752. URL: https://link.aps.org/doi/10.1103/PhysRevD.15.2752.

[51] Ian Jubb et al. "Boundary and corner terms in the action for general relativity". In: *Classical and Quantum Gravity* 34.6 (Feb. 2017), p. 065006. DOI: 10.1088/1361-6382/aa6014. URL: https://doi.org/10.1088%2F1361-6382%2Faa6014.

[52] Eric W. Weisstein. *Circle-Circle Intersection*. 21 September 2023. 2023. URL: https://mathworld.wolfram.com/Circle-CircleIntersection.html.

[53] Djamel Dou and Rafael D Sorkin. "Black-hole entropy as causal links". In: *Foundations of Physics* 33 (2003), pp. 279–296.

[54] Ludovico Machet and Jinzhao Wang. "On the horizon entropy of a causal set". In: *Classical and Quantum Gravity* 38.8 (2021), p. 085004.

[55] Sumati Surya. "Evidence for the continuum in 2D causal set quantum gravity". In: *Classical and Quantum Gravity* 29.13 (June 2012), p. 132001. DOI: 10.1088/0264-9381/29/13/132001. URL: https://doi.org/10.1088%2F0264-9381%2F29%2F13%2F132001.

[56] William J Cunningham and Sumati Surya. "Dimensionally restricted causal set quantum gravity: examples in two and three dimensions". In: *Classical and Quantum Gravity* 37.5 (Feb. 2020), p. 054002. DOI: 10.1088/1361-6382/ab60b7. URL: https://doi.org/10.1088%2F1361-6382%2Fab60b7.